LAWRENCE
LIVERMORE
NATIONAL
LABORATORY

LLNL-TR-763329

FY18 LLNL Experimental Programs at Omega

R. F. Heeter, S. J. Ali, L. R. Benedetti, J. V. Bernier, H. Chen, F. Coppari, L. Elgin, A. Fernandez-Panella, E. Gumbrell, R. Hua, C. M. Huntington, S. Jiang, G. E. Kemp, S. F. Khan, A. Krygier, C. Kuranz, A. E. Lazicki, N. Lemos, M. J. MacDonald, D. Mariscal, E. V. Marley, M. C. Marshall, D. A. Martinez, J. M. McNaney, M. A. Millot, Y. Ping, B. B. Pollock, P. L. Poole, H. G. Rinderknecht, M. Rubery, A. M. Saunders, R. F. Smith, G. F. Swadling, R. Tommasini, K. Widmann, G. J. Williams, O. L. Landen, W. W. Hsing, A. S. Wan

November 30, 2018

Disclaimer

This work performed under the auspices of the U.S. Department of Energy by Lawrence Livermore National Laboratory under Contract DE-AC52-07NA27344.

FY18 LLNL Experimental Programs at Omega

R. F. Heeter, S. J. Ali, L. R. Benedetti, J. V. Bernier, H. Chen, F. Coppari, L. Elgin, A. Fernandez-Panella, E. Gumbrell, R. Hua, C. M. Huntington, S. Jiang, G. E. Kemp, S. F. Khan, A. Krygier, C. Kuranz, A. E. Lazicki, N. Lemos, M. J. MacDonald, D. Mariscal, E. V. Marley, M. C. Marshall, D. A. Martinez, J. M. McNaney, M. A. Millot, Y. Ping, B. B. Pollock, P. L. Poole, H. G. Rinderknecht, M. Rubery, A. M. Saunders, R. F. Smith, G. F. Swadling, R. Tommasini, K. Widmann, G. J. Williams, O. L. Landen, W. W. Hsing, A. S. Wan

November 28, 2018

This work performed under the auspices of the U.S. Department of Energy by Lawrence Livermore National Laboratory under Contract DE-AC52-07NA27344.

FY18 LLNL Experimental Programs at Omega

R.F. Heeter, S.J. Ali, L.R. Benedetti, J.V. Bernier, H. Chen, F. Coppari, L. Elgin (U Michigan), A. Fernandez Panella, E. Gumbrell (AWE), R. Hua (UCSD), C.M. Huntington, S. Jiang, G.E. Kemp, S.F. Khan, A. Krygier, C. Kuranz (U Michigan), A.E. Lazicki, N. Lemos, M.J. MacDonald, D. Mariscal, E.V. Marley, M.C. Marshall (formerly M.C. Gregor), D.A. Martinez, J.M. McNaney, M.A. Millot, Y. Ping, B.B. Pollock, P.L. Poole, H.G. Rinderknecht (now LLE), M. Rubery (AWE), A.M. Saunders, R.F. Smith, G.F. Swadling, R. Tommasini, K. Widmann, G.J. Williams, O.L. Landen, W.W. Hsing and A.S. Wan

In Fiscal Year 2018 (FY18), Lawrence Livermore National Laboratory's (LLNL's) High-Energy-Density Physics (HED) and Indirect Drive Inertial Confinement Fusion (ICF-ID) programs conducted numerous campaigns on the OMEGA and OMEGA-EP (EP) laser systems. This was the 20th year of National Lab collaborative experiments at OMEGA since the Nova Laser at LLNL shut down in 1999 [1], building upon prior collaborations. In FY18 overall, these LLNL programs led 465 target shots, with 283 shots using just the OMEGA laser system, 172 shots using just the EP laser system, and 10 Joint shots using both lasers together. Approximately 28% of the total number of shots (60 OMEGA shots and 71 EP shots) supported the Indirect Drive Inertial Confinement Fusion Campaign. The remaining 72% (223 OMEGA-only shots, 101 EP-only shots and 10 Joint shots) were dedicated to experiments for High-Energy-Density Physics. Highlights of the various HED and ICF-ID campaigns are summarized in the following reports.

In addition to these experiments, LLNL Principal Investigators (PIs) led a variety of Laboratory Basic Science campaigns using OMEGA and EP, including 99 target shots using just OMEGA and 39 shots using just EP. The highlights of these are also summarized, following the ICF and HED campaigns.

Overall, LLNL PIs led a total of 603 shots at LLE in FY 2018. In addition, LLNL PIs supported 47 NLUF shots on Omega and 31 NLUF shots on EP in collaboration with the academic community.

[1] LLE 1999 Annual Report, DOE/SF/19460-332 (January 2000). This report notes on page 222 that LLNL conducted 173 shots on OMEGA in 1999.

This work performed under the auspices of the U.S. Department of Energy by Lawrence Livermore National Laboratory under Contract DE-AC52-07NA27344.

Table of Contents

Indirect Drive Inertial Confinement Fusion Experiments

1. Short-Pulse Backlighters Using In-Situ Plasma Reflectors (PI: R. Tommasini)

with J. Park, L. Divol and A. Kemp

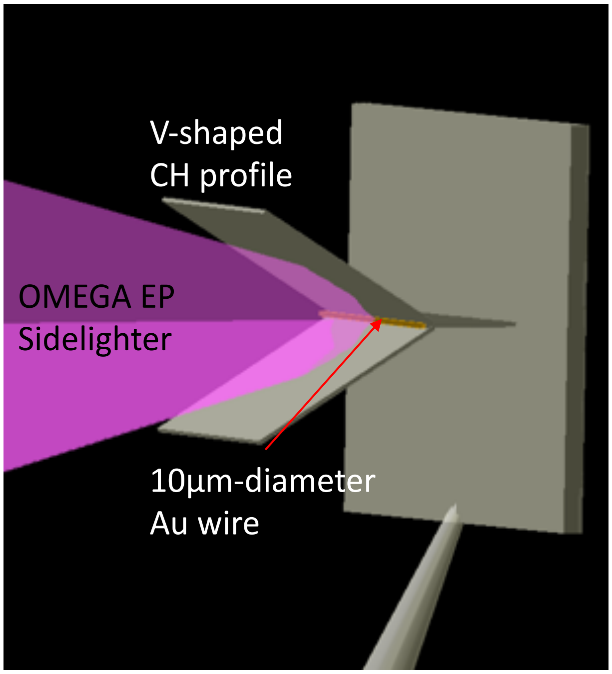

Figure 1. Experimental configuration for Omega-EP shot 79708.

The SmallSpotBL-EP campaign was designed to test novel small source x-ray backlighters. The design uses in-situ plasma mirrors to enhance the laser energy coupling on the backlighter target and thereby increase the conversion efficiency into x-rays and, at the same time, mitigate the issue of pointing the laser spot onto backlighters small enough to act as point sources.

The targets, shown in Figure 1, consisted of 10 micron diameter gold wires placed at the vertex of a v-shaped profile formed by two CH foils. The angle between the two foils was chosen to be 40 or 60 degrees. The Omega-EP sidelighter beam delivered 30 ps, 1 kJ pulses into the vertex. The x-ray yield and source size were measured, along the line of sight parallel with the gold wire, by radiographing a tantalum step-wedge and a calibrated 200 micron diameter tungsten sphere.

Shots with and without the v-shaped profile were performed and compared. The results have fully proved the concept: X-ray conversion efficiency increased ~3x using the plasma mirror configuration as compared to bare wires, with great reproducibility and also a 25% reduction in source size. The results have validated a similar experiment performed earlier on NIF-ARC. An improved version of these backlighters, employing parabolic-like shaped profiles, has been designed and will be tested in the upcoming experiments on Omega-EP.

These novel schemes open the way to the next generation of backlighters to be used for hard-x-ray radiography of the dense cores in ICF implosions and will allow the reduction of the backlighter size in order to record radiographs with sufficient signal to noise and higher spatial resolution.

2. Diamond Sound Speed Measurements Between 8-14 Mbar (PI: A. Fernandez-Panella)

with D. Fratanduono and P. Celliers

This half day at OMEGA was designed to constrain equation of state models by collecting high quality data on the sound speed of diamond in the multi Mbar range. The FY18 shots completed the dataset from the previous FY17 campaign where 4 data points were acquired up to 13 Mbar.

The campaign used planar targets and a direct-drive configuration with CH or Be ablator, a quartz pusher and two targets side by side: quartz (standard) and diamond. The velocity profiles at the free surface were recorded using VISAR as the primary diagnostic (Figure 1). The laser drive energy was varied to probe different shocked pressure states in diamond. The laser pulse was designed to produce a small pressure perturbation that propagated through both the standard and the sample. Then the wave propagation analysis described in [1] was applied to extract the sound speed of both materials, quartz and diamond, from their velocity profiles (Figure 2).

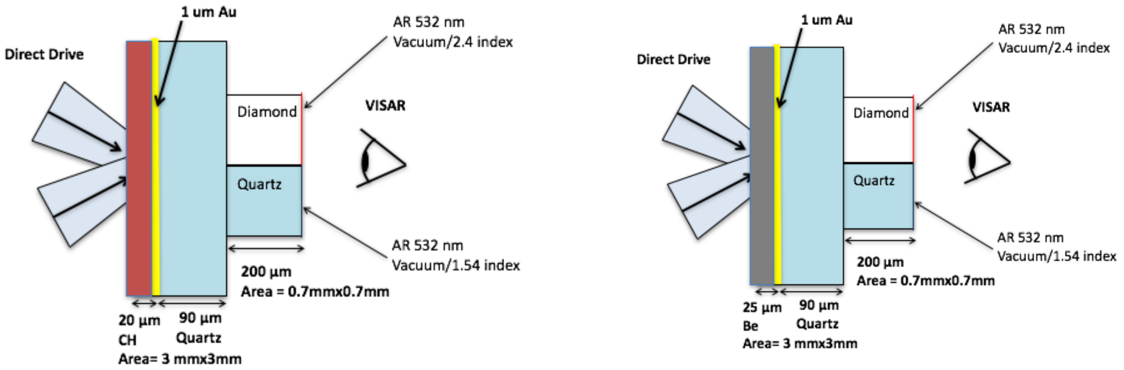

Figure 1. Experimental setup and target designs (CH and Be ablators) for DiamondSS-18A campaign.

This campaign produced 7 good data points from 700–1800 GPa. The data analysis is still in progress. The position in pressure of the data acquired in FY18 campaign are signaled by blue circles in Figure 2, where filled circles and open circles represent data obtained by using CH and Be ablators respectively. The results from the previous FY17 shots were useful to optimize the target design, VISAR etalon choice and so on, and they indicate that sound speed measurements are sensitive enough to constrain EOS models. The Livermore LEOS table 9061 shows good agreement with the data. The full analysis of the campaign data set should be able to constrain the EOS models in a wide pressure range up to 20 Mbar.

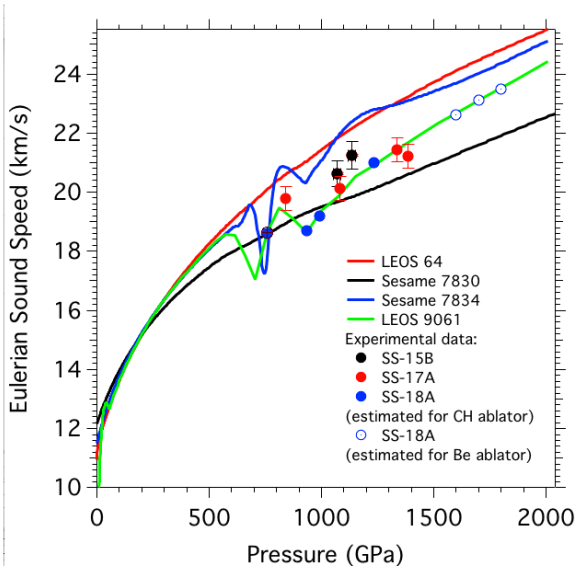

Figure 2. Diamond sound speed versus pressure.

[1] D. Fratanduono *et al.*, *Journal of Applied Physics* **116**, 033517 (2014).

3. Thomson Scattering Measurements from Gold- and Beryllium-Coated Spheres (PI: G.F. Swadling)

with J. S. Ross, M. Rosen, K. Widmann and J. Moody

The AuSphereInFoam campaign sought to collect data using the foam-covered sphere platform developed for the FoamCoSphere day in FY17. Additional aims were to carry out burn-through measurements using thin wall (100 – 400 nm) gold sphere targets, and measurements of Be coated targets to provide benchmarking data for rad-hydro models in a regime less dominated by complex atomic physics of gold.

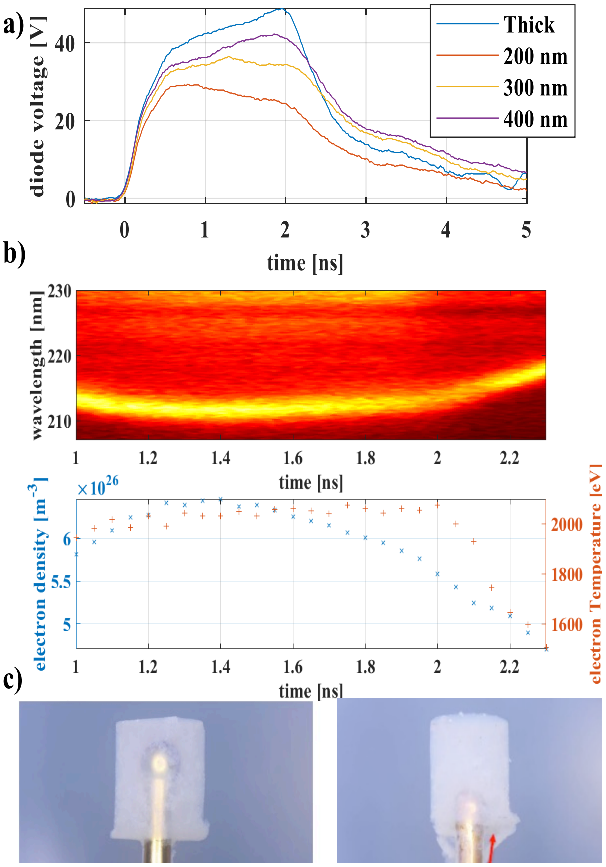

Figure 3. (a) Dante trace showing change in soft x-ray emission with gold thickness for 2ns heater pulse. (b) Thomson scattering data fitted to extract T_e, n_e vs time for Be coated target. (c) Examples of 2 foam covered targets, showing variation in centering, shape and size.

On this platform spherical targets are symmetrically heated using the 60 OMEGA beams in spherical geometry to investigate atomic physics models, radiative properties of the laser spot plasma, and the interpenetration of multi-ion species plasmas relevant to ICF indirect drive ignition hohlraums. These experiments use a laser irradiation of 10^{14} to 10^{15} W/cm^2, similar to the intensities found in ICF hohlraums fielded on the NIF.

The thin wall target experiments used 0.86 mm diameter spheres with variable coating thicknesses. The spheres were heated using either 1 or 2 ns laser pulses. The plasma temperature and density were measured at various radial positions in the blow-off plasma using Thomson scattering (TS), while x-ray flux from the gold sphere was recorded using the DANTE soft x-ray spectrometer. These shots were very successful; the data appears to be highly reproducible and the trends are consistent with pre-shot modeling (Figure a). The data captured in these experiments is currently being used to benchmark transport models.

The Be Sphere shots also produced high quality TS data which has been fit using theoretical curves to produce accurate measurements of blow-off plasma density and temperature (Figure b). A shot day in FY19 is planned to further benchmark non-local transport models.

Finally, in the foam-covered sphere experiments the Au sphere was embedded in a low-density (3.8 mg/cc) CH foam. Inconsistencies in the centration of the sphere with respect to the foam, combined with irregularities in the foam shape and suspected density-clumping within the foam (Figure c) led to data which was not reproducible shot-to-shot. The technical issues with foam fabrication are related to its very low density and the absence of a surrounding support structure in these open geometry targets. Additional target fabrication improvements are required before this type of target can be fielded for detailed scientific studies.

4. Hydrodynamic Response from Non-Uniformities in High-Density Carbon, Plastic and Beryllium Ablators (PI: S. Ali)

with P. M. Celliers, S. W. Haan, S. Baxamusa, H. Reynolds, M. Johnson, H. Xu, N. Alexander, H. Huang, V. Smalyuk, H. Robey

Performance and yield from fusion capsules at the National Ignition Facility (NIF) are highly dependent on the uniformity of the capsule implosion, and hydrodynamic instabilities are a significant source of performance degradation during the implosion. These can arise due to, among other reasons, intrinsic heterogeneity within the capsule material. Beryllium and high-density carbon (HDC) have complex microstructures, and both are acoustically anisotropic, which can lead to variations in the shock speed in crystallites of different orientations, potentially seeding instabilities. Additional sources of heterogeneous response include behavior of the grain boundary material, which is often of a different bonding character than the crystallites, voids in the deposited material, and static internal stresses in the polycrystalline structure. The current strategy for reducing the impact of internal heterogeneities is to fully melt the ablator material on the first shock, requiring 2.6 Mbar for beryllium and >12 Mbar for HDC.[1-4] In the case of HDC this strong shock also raises the entropy of the fuel, making it more difficult to reach the high densities required for ignition. As part of the effort to understand both the origin and impact of the velocity non-uniformities in all three ablators, this campaign conducted two-dimensional velocimetry experiments on planar foils of the three ablator materials under conditions near the first shock and second shock level in beryllium and GDP, and up to the first shock level in HDC.

The Capseed campaign goal is to measure shock front velocity non-uniformities in Inertial Confinement Fusion (ICF) ablator materials and quantify the level of non-uniformity caused by intrinsic effects. This is done using the Omega High Resolution Velocimeter (OHRV) to obtain velocity maps of the optically reflecting shock front following release of the ablator material into either PMMA for the warm experiments or cryogenic deuterium for the cryo experiments.

There were three Capseed campaigns in FY18: CapseedHDC, Capseed2ShockCryo, and CapseedShellCryo. The goal of CapseedHDC was to obtain a pressure scan of velocity nonuniformity over the HDC melt region, 7 to 12 Mbar, helping constrain the first shock level required for a uniform shock response. The warm component of CapseedHDC also included measurements of the fill tube perturbation from 5, 10, and 30 micron diameter fill tubes, with perturbation sizes comparing qualitatively well with simulations. Capseed2ShockCryo was used to investigate velocity nonuniformity growth on transit of a second shock through GDP and Be. While relatively little nonuniformity increase was seen in the GDP, the RMS for second shock Be increased by a factor of three. CapseedShellCryo was an initial attempt to move toward more capsule-like targets, as opposed to the planar foils that have been used for past Capseed campaigns, by using segments from large diameter (4.5-5 mm) capsules, beginning with a successful experiment on 5 mm diameter GDP hemispheres on the first half-day. Unfortunately, due to fabrication delays, the 5 mm HDC spheres were not complete in time for the second half-day, but a secondary goal of measuring the effect of grain size on the nonuniformity was achieved. A significant improvement was seen in the velocity RMS for the nanocrystalline vs. microcrystalline samples, as shown in Figure 1. These experiments are continuing into FY19, with two half-days of further cryogenic measurements planned.

[1] D. K. Bradley, S. T. Prisbrey, R. H. Page, D. G. Braun, M. J. Edwards, R. Hibbard, K. A. Moreno, M. P. Mauldin and A. Nikroo, Phys. Plasmas **16** (2009).
[2] D. K. Bradley, J. H. Eggert, R. F. Smith, S. T. Prisbrey, D. G. Hicks, D. G. Braun, J. Biener, A. V. Hamza, R. E. Rudd and G. W. Collins, Phys. Rev. Lett. **102** (2009).
[3] S. W. Haan, J. D. Lindl, D. A. Callahan, D. S. Clark, J. D. Salmonson, B. A. Hammel, L. J. Atherton, R. C. Cook, M. J. Edwards, S. Glenzer *et al.*, Phys. Plasmas **18** (2011).
[4] L. X. Benedict, K. P. Driver, S. Hamel, B. Militzer, T. T. Qi, A. A. Correa, A. Saul and E. Schwegler, Phys Rev B **89** (2014).

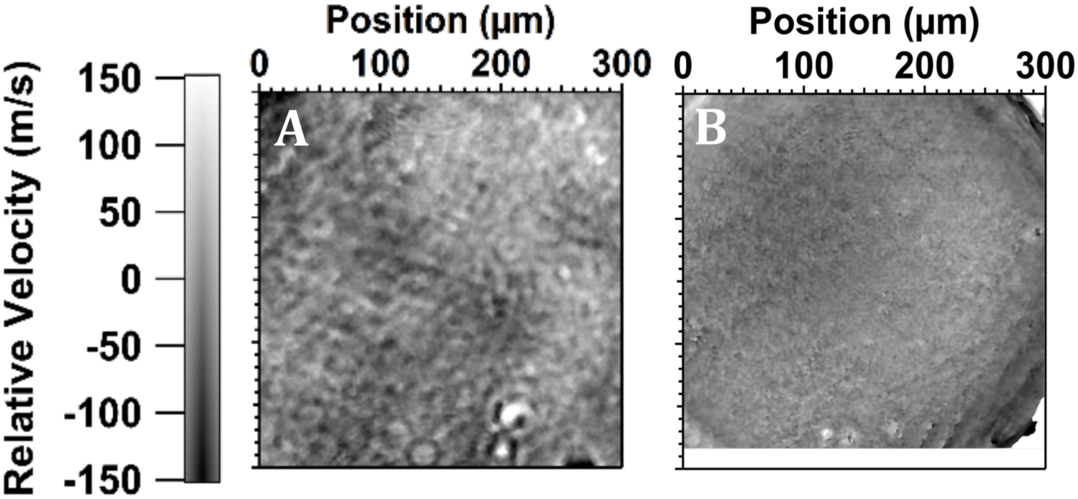

Figure 1. Velocity maps from microcrystalline (A) and nanocrystalline (B) HDC releasing into D2 at 12 Mbar. RMS velocity roughness was 35 m/s for (A) and 11 m/s for (B), with diagnostic detection limits of 10 m/s (A) and 5 m/s for (B).

5. Near-Critical-Density X-ray and Particle Sources (PI: N. Lemos)

with A. Pak, A. Kemp, G.J. Williams, D. Mariscal, O.L. Landen and T. Ma

A series of shots was designed to understand how to increase the x-ray/proton yield using near critical density targets at ARC [1] relevant pulse durations/intensities. These shots maximized the ion and x-ray emission by optimizing the scale length of the pre-plasma in front of the solid target.

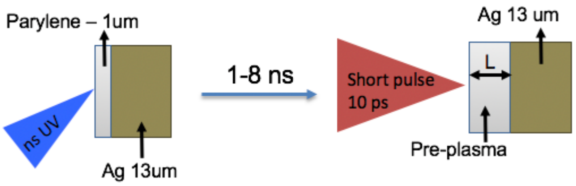

Figure 1: Experimental setup

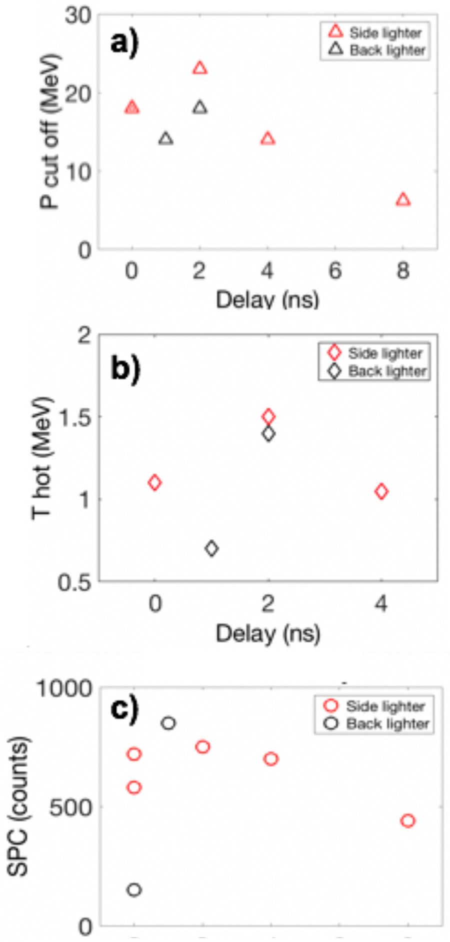

Figure 2: (a) Maximum proton energy, (b) electron temperature and (c) x-ray yield vs delay between the long and short pulse.

Results obtained on OMEGA EP [2, 3] and recent results from LFEX (Osaka University) [4] have shown that by extending the laser pulse duration to several picoseconds, the maximum proton energy produced by the Target Normal Sheath Acceleration (TNSA) mechanism more than doubled. This enhanced energy and efficiency exceeds the theoretical prediction given by the standard target normal sheath acceleration theory, and particle-in-cell (PIC) simulations. These experiments show that a superponderomotive electron distribution generated by the ps-scale laser pulses drives an increase to the maximum sheath potential.

The present experiment combined the advantages of the long pulse duration to enhance the TNSA fields, and increased laser absorption with a pre-plasma in front of the target. A controlled pre-plasma was produced by focusing a 10J, 10ns UV laser pulse onto a parylene-coated, 13um Silver foil prior to the arrival of the high-intensity ARC like beam (Fig. 1). The short pulse beam was delayed 1-8 ns relative to the UV beam.

Figure 2a) shows the maximum proton energy (22 MeV) was achieved with a 2 ns delay between the two pulses; increasing the delay further degraded the performance. Fig. 2b) shows the escaped electron temperature is also maximized at a delay of 2ns and corroborates the result shown in figure 2a). Figure 2c) also shows the maximum x-ray yield at a delay of 1-2ns, indicating this delay is where the laser is better coupled into the solid target.

Results of this campaign are being used to optimize a similar platform that is being develop at NIF-ARC.

[1] J. K. Crane, et. al., Phys.: Conf. Ser. 244, 032003 (2010)
[2] Gao, L. *et al.* Measurements of proton generation with intense, kilojoule laser pulses on OMEGA EP. *Bull. Am. Phys. Soc.* **55(15)** (2010).
[3] J. Peebles, et. al. "Investigation of laser pulse length and pre-plasma scale length impact on hot electron generation on OMEGA-EP", New J. Phys. 19 (2017) 023008
[4] A. Yogo, et al "Boosting laser-ion acceleration with multi-picosecond pulses", Sci Rep. 2017 Feb 13;7:42451. doi: 10.1038/srep42451

6. Optimization Study of Thin-Foil Backlighters for Use on NIF-ARC (PI: G. J. Williams)

with H. Chen, A. Kemp, N. Candeias Lemos, T. Ma, D. Mariscal and O.L. Landen

This series of shots was designed to benchmark backlighter conversion efficiency for NIF-ARC conditions [1] for various pulse durations and intensities, with 1D x-ray source size measurements for side-on radiography applications. Electron temperatures and K-alpha line emissions were measured across a laser and target parameter scan.

Recent simulation and experimental work have shown that, for a given power or intensity, the electron temperature continues to increase with pulse duration up to a saturation limit dependent on the spot size [2-4]. Underdense plasma will one-dimensionally expand from the target front surface until the scale length exceeds the spot size. At ARC-like conditions, the large spot size is invoked to explain the observed relativistic electrons despite an intensity of 10^{18} W/cm^2 [5]. The electron temperature is fundamental to optimizing high energy x-ray backlighters.

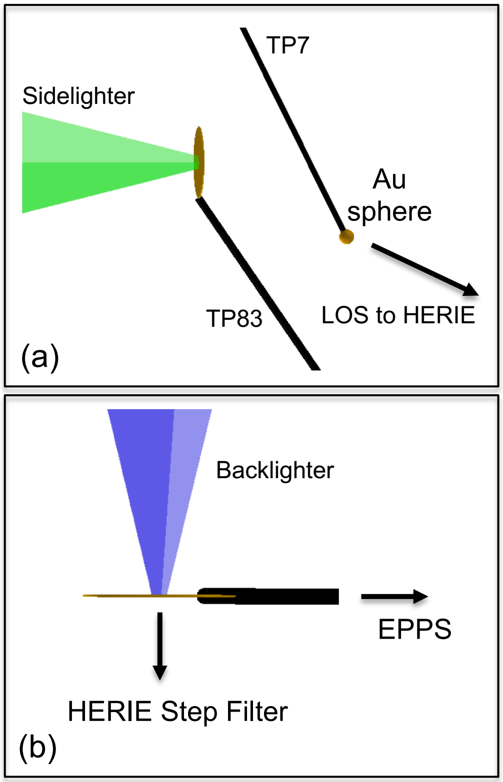

Figure 1: Experimental configuration for (a) Sidelighter and (b) Backlighter

Interleaved short pulse shots were performed on Omega EP using 5 and 15 um gold foil targets with a 1 micron CH tamper layer. In the Beam 1 (Sidelighter) configuration, a gold sphere is used to project a shadow of the x-ray source perpendicular to the foil, as shown in Fig. 1a, with a near-constant energy on target at pulse durations of 3, 10, and 30 ps. The Beam 2 (Backlighter) shots used a fixed intensity of 10^{18} W/cm^2 by changing both energy and pulse duration together (see Fig. 1b).

Measurements of x-rays and electrons were recorded for all shots. In line with expectations, the data show an increase and then saturation of the electron temperature with pulse duration for a fixed intensity (Fig. 2a). A correlation to existing scaling for underdense electron acceleration [6] was observed by scanning over a range of laser powers (intensities), where the Pukhov scaling of $kT \sim \sqrt{I/I_{18}}$ is shown with electron data in Fig. 2b. The Au K-alpha x-ray yield scaled linearly with pulse duration for a given target but did not correlate with intensity (Fig. 2c). X-ray source size measurements are ongoing; data suggests x-rays >20 keV have a source 1.5-2.5 times that of the foil thickness. This measurement could be influenced by the plasma blowoff and the softer filtering used. The results of this campaign will be used to optimize the performance of future NIF-ARC x-ray backlighter platforms.

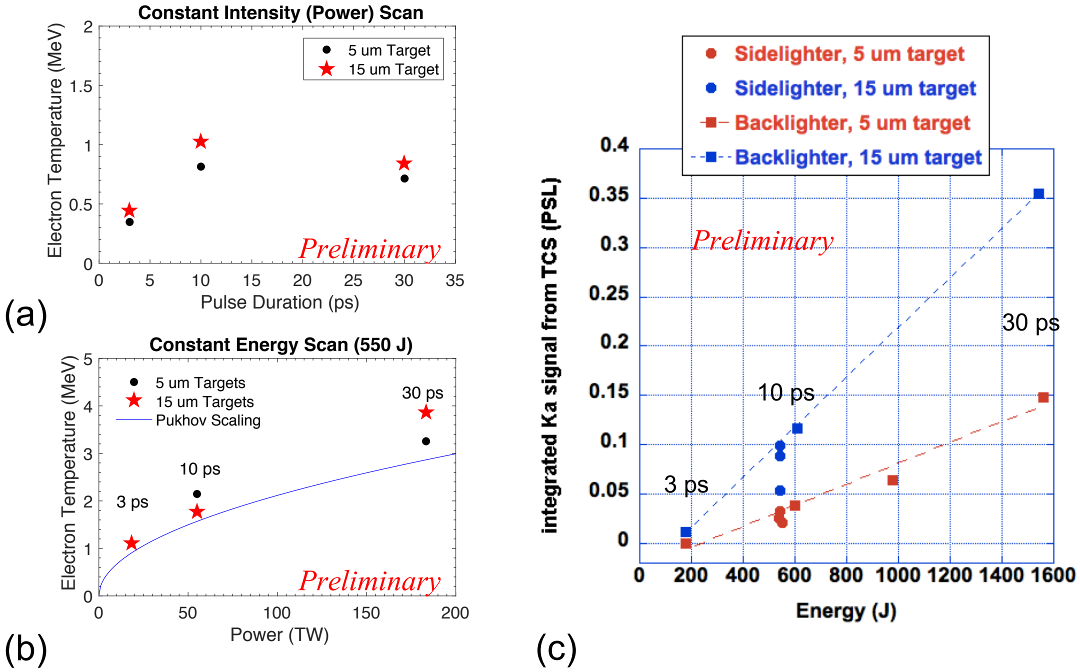

Figure 2: Electron temperature measurements at (a) constant power and (b) constant intensity. (c) X-ray K-alpha yields for all shots.

[1] Hui Chen, M. R. Hermann, D. H. Kalantar, D. A. Martinez, P. Di Nicola, R. Tommasini, O. L. Landen, D. Alessi, M. Bowers, D. Browning, G. Brunton, T. Budge, J. Crane, J.-M. Di Nicola, T. D¨oppner, S. Dixit, G. Erbert, B. Fishler, J. Halpin, M. Hamamoto, J. Heebner, V. J. Hernandez, M. Hohenberger, D. Homoelle, J. Honig, W. Hsing, N. Izumi, S. Khan, K. LaFortune, J. Lawson, S. R. Nagel, R. A. Negres, L. Novikova, C. Orth, L. Pelz, M. Prantil, M. Rushford, M. Shaw, M. Sherlock, R. Sigurdsson, P. Wegner, C. Widmayer, G. J. Williams, W. Williams, P. Whitman, and S. Yang. High-energy (>70 kev) x-ray conversion efficiency measurement on the ARC laser at the National Ignition Facility. *Physics of Plasmas*, 24(3):033112, 2017.

[2] A. J. Kemp and L. Divol. Interaction physics of multipicosecond petawatt laser pulses with overdense plasma. *Phys. Rev. Lett.*, 109:195005, Nov 2012.

[3] A. Yogo, K. Mima, N. Iwata, S. Tosaki, A. Morace, Y. Arikawa, S. Fujioka, T. Johzaki, Y. Sentoku, H. Nishimura, A. Sagisaka, K. Matsuo, N. Kamitsukasa, S. Kojima, H. Nagatomo, M. Nakai, H. Shi- raga, M. Murakami, S. Tokita, J. Kawanaka, N. Miyanaga, K. Yamanoi, T. Norimatsu, H. Sakagami, S. V. Bulanov, K. Kondo, and H. Azechi. Boosting laser-ion acceleration with multi-picosecond pulses. *Scientific Reports*, 7:42451 EP, 02 2017.

[4] N. Iwata, K Mima, Y. Sentoku, A. Yogo, H. Nagatomo, H Nishimura, and H. Azechi. Fast ion acceleration in a foil plasma heated by a multi-picosecond high intensity laser. *Physics of Plasmas*, 24(7):073111, 2017.

[5] J. Kim, A. J. Kemp, S. C. Wilks, D. H. Kalantar, S. Kerr, D. Mariscal, F. N. Beg, C. McGuffey, and T. Ma. Computational modeling of proton acceleration with multi-picosecond and high energy, kilojoule, lasers. *Physics of Plasmas*, 25(8):083109, 2018.

[6] G. J. Williams, H. Chen, D. A. Alessi, G. Fiksel, F. Fiuza, M. R. Hermann, E. d'Humires, D. Kalantar, A. Kemp, S. Kerr, A. Link, T. Ma, D. A. Mariscal, D. Martinez, B. Remington, R. Sigurdsson, W. Williams, L. Willingale, and R. Zachariason. Relativistic electron production using the NIF-ARC laser. *Phys Rev Lett*, In Preparation, 2018.

[7] A. Pukhov, Z.-M. Sheng, and J. Meyer-ter Vehn. Particle acceleration in relativistic laser channels. *Phys. Plasmas*, 6(7):2847–2854, 1999.

7. Characterization of Laser-Driven Magnetic Fields (PI: B.B. Pollock)

with C. Goyon, J. Williams, D. Mariscal, G. Swadling, J.S. Ross, and J.D. Moody (LLNL), in collaboration with S. Fujioka, H. Morita, and K. Law (Osaka University)

Two shot days on Omega-EP continued the laser-driven magnetic field experimental campaign. The goals for FY18 were to study the magnetic field generation and decay at times late compared to previous experiments (>1 ns), while also expanding the measurement capability of the spatial profile of the magnetic field.

Figure 1 shows the general experimental geometry for the BFieldLoop experimental campaigns. The field is produced by currents flowing in the Au U-shaped foil target. Long pulse beams are directed through the holes in the front side of the target to produce a plasma on its interior rear side. Plasma produced in this region expands toward the front side, setting up a voltage across the target which drives current and produces magnetic field. The field is measured by proton deflectometry in the fringing field outside the U, and in the high-field region inside the U through hole/slot pairs in the target surfaces where the flat-to-curved transition occurs. The protons are produced through Target-Normal Sheath Acceleration by the BL on a thin Au foil.

Previous experiments demonstrated that for 1 TW long-pulse laser drive, fields of ~200 T can be produced in the interior of the loop portion of the target in ~1 ns. The first FY18 experiment looked at the evolution of the magnetic field at later times, though while the drive pulse was still on. These measurements from 3 to 10 ns showed that the field continued to increase while the 0.5 TW long-pulse drive remained on, albeit at a slower rate than expected in the first nanosecond. The second experiment repeated some of these measurements, but also looked again at time <1 ns with a reduced 0.5 TW drive beam power (compared to 1 TW in previous shot days). Additionally, these targets added two more hole/slot pairs along the target length, to enable measurement of the axial uniformity of the field inside the target.

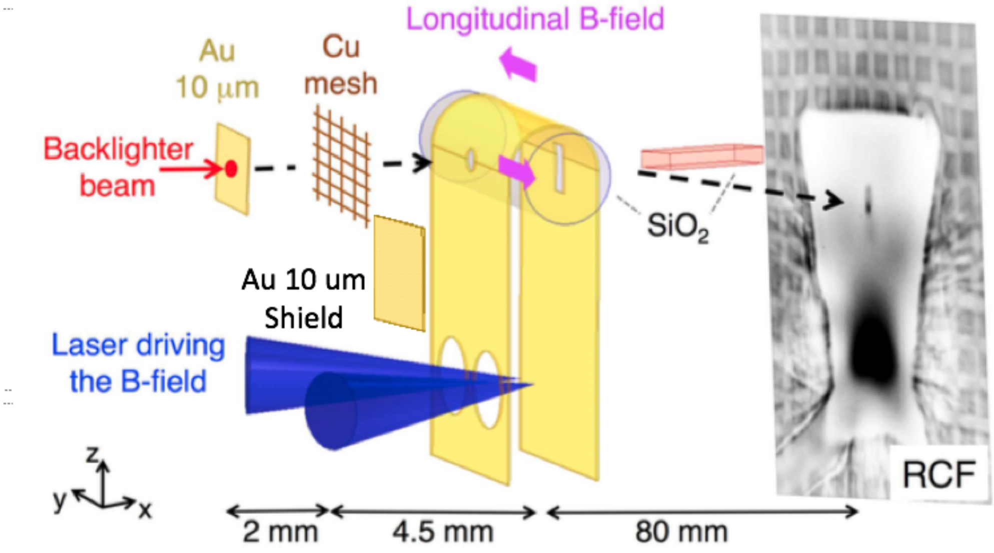

Figure 1. Experimental configuration for BFieldLoop experiments.

The field measurements from the second day do show a faster rise of the magnetic field during the first 1 ns of the drive. The slope by 3 ns has become much less steep, even though it appears the field continues to increase thereafter as seen in the first day. The representation of this target as a lumped-element circuit with a constant voltage implied a linear ramp in the current with respect to time. The finding of a slope change may drive a different interpretation at later times, but substantial additional analysis is still needed. Furthermore, the proton measurements of the field inside the target seem to indicate that the field is asymmetric along the target length. Improved modeling of the current distribution is underway to assess this observation, and there are several experimental methods available to test the controllability of this behavior if it is borne out by modeling. Other hypotheses include target deformation during the drive, but this again will require additional investigation.

8. Study of Shock Fronts in Low-Density Single- and Multi-Species Systems (PI: R. Hua, UCSD)

with Y. Ping (LLNL), H. Sio (MIT), S. C. Wilks (LLNL), C. McGuffey (UCSD), M. Bailly-Grandvaux (UCSD), F. N. Beg (UCSD), G. W. Collins (LLNL, LLE), R.F. Heeter (LLNL) and J.A. Emig (LLNL)

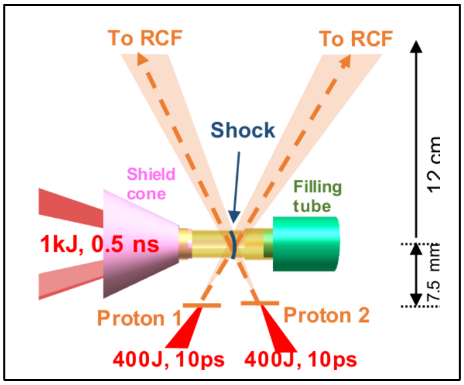

Figure 1. Experimental configuration.

This series of shots studied the plasma shock structure, especially the associated field structure, of single and multi-species in low-density system under a planar geometry using TNSA protons and X-ray spectroscopy. Two or three synchronized long pulse beams from EP delivered a couple of kilojoules total energy in a few nanoseconds onto a 2 micron SiO_2 foil that pushed into pure helium or mixed (helium and neon) gases, thus initiating strong shocks. A short pulse of 400 joules in 10 picoseconds illuminated a side-on copper foil a few nanoseconds after the shock creation, creating a burst of protons that probed the propagating shock through two 1 micron windows along the tube. The protons with energies spanning ~ 20 MeV were collected by a radiochromic film stack. The relative position from the proton source to the shock front was varied intentionally to distinguish magnetic from electric field effects. A 1-D resolved X-ray spectrometer recorded the emission from the shock front for the inference of temperature and density. The details of the design and its feasibility have been published [1].

The contrary proton deflection pattern, higher flux ahead (bright ring) or lower flux ahead (dark) ring, from two source positions confirm the domination of magnetic field at the shock front, since electric fields deflect protons in a manner that is independent of incident angle. Details of this analysis has been submitted recently. Data analysis of a shock in multi-species composed of 90% helium and 10% neon is in progress. In this shot, radiography data shows a double peak of proton flux at the shock front, indicating more complex field structures. The added neon gas provided useful data for the 1-D resolved spectroscopy, allowing the inference of density and temperature profiles along the shock propagation direction. In addition, spatial correlation between the RCF and X-ray data was achieved from the designed spatial references.

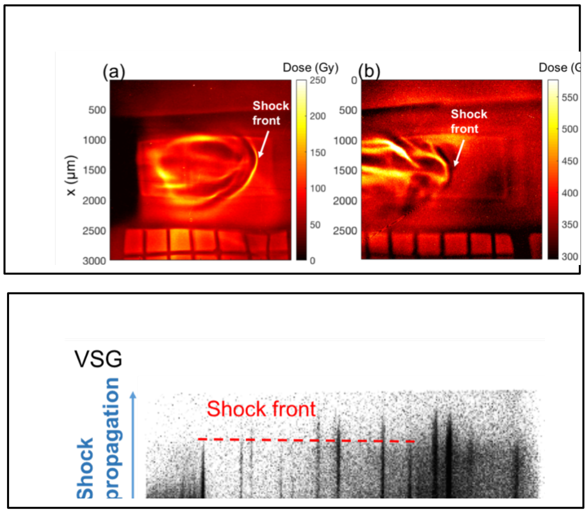

Figure 2. Raw radiographs and 1-D resolved spectrum.

[1] H. Sio, *et al.* Rev. Sci. Instrum. **88**, 013503 (2017).

High-Energy-Density Experiments

A. Material Equation of State and Strength Measured Using Diffraction

1. X-Ray Diffraction of Ramp-Compressed Copper Up To 1.2 TPa

(PI: A. Fernandez-Panella)

with R. F. Smith, J. K. Wicks, D. E. Fratanduono and J. H. Eggert.

Copper is an abundant element that has been extensively studied, both experimentally and theoretically, by itself and within the different alloys it forms. It is also commonly used as a pressure standard, flyer plate and ablator material within the high-pressure community. Its electronic structure is simple with the 3d shell completely filled, accurate shock wave and ramp-compression data is available up to a few Mbar [1-5], and copper's FCC phase structure is predicted to remain stable up to very high pressures [6].

Along the Hugoniot, Cu melts above 200 GPa. To determine its stable solid phase structure at higher pressures, a low-temperature off-Hugoniot compression path is required. The purpose of the CuDiff-18B campaign was to measure x-ray diffraction data of ramp-compressed Cu up to 1.2 TPa. An example of an x-ray diffraction data at 1165 GA is shown in Fig.1. The results are summarized in Fig 2. They indicate that along the isotherm copper remains in the FCC phase structure up to the highest pressures explored in this study, 1.2 TPa. These results supplement the recent EOS ramp-compressed data measured at the National Ignition facility up to 2.4 TPa [7] and have been included in the manuscript for publication.

[1] H. K. Mao *et al.*, J. Appl. Phys 1978, **49**, 3276.
[2] A. D. Chijioke *et* al., J. Appl. Phys. 2005, **98**, 073526.
[3] Y. Wang *et al.*, J. Appl. Phys. 2002, **92**, 6616.
[4] A. Dewaele *et al.*, Phys. Rev. B 2004, **70**, 094112.
[5] R. G. Kraus *et al.*, Phys. Rev. B 2016, **93**, 134105.
[6] C. W. Greeff *et al..,* J. Phys. Chem. of solids 2006, 67, M. Svandrlik, F. Parmigiani, *Nat. Photonics* 2014, **8,** 82.
[7] R. F. Smith, private communication.

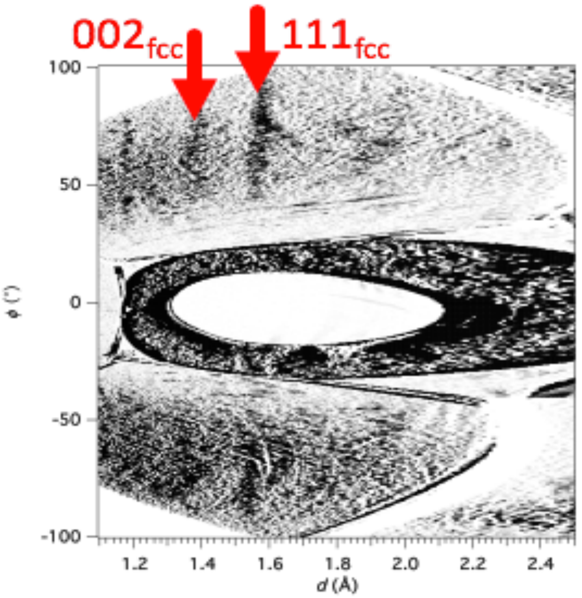

Figure 1. X-ray diffraction measurement of ramp compressed Cu at 1165 GPa. The observed lines (marked with red arrows) correspond to the fcc phase structure.

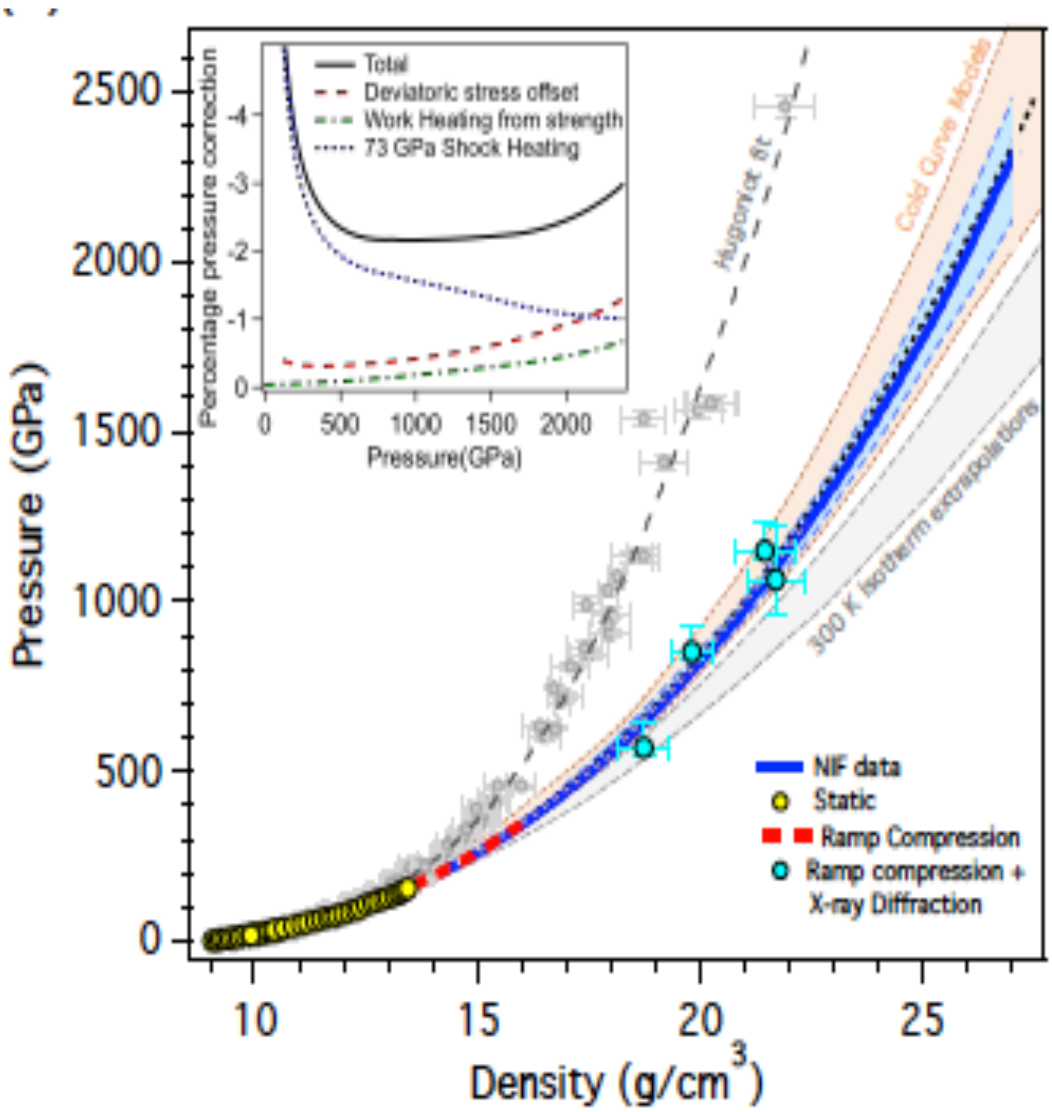

Figure 2. Pressure-density plot of copper. Hugoniot data [3], ramp compressed (red [5] and blue curves [7]), and several theoretical cold curves (dashed grey lines) and the extrapolated isotherm at 300 K (solid grey line) are shown. The corresponding fcc pressure states measured at the Omega Laser are indicated with filled blue circles.

2. Examination of the High-Pressure Structures of Ramp-Compressed Germanium and Zirconium (PI: J.V. Bernier)

with R. Kraus, C. Wehrenberg, A. Krygier, and J. Eggert

This campaign was designed to quantify the hydrodynamic responses and high-pressure crystal structures in both Germanium and Zirconium subject to ramp compression. Both of these materials are commonly used as X-ray backlighter sources (He-α) across the HED campaigns, and they are also used as filter layers in physics packages. There is, however, a dearth of data regarding the crystal structures in these materials at moderately high pressures relevant to many ramp-compression experiments. The specific objectives were: 1) to assess the fidelity of the modeled hydrodynamic responses (as a check on the available EOS's); and 2) to measure the high-pressure structures of both materials via diffraction patterns measured on the PXRDIP diagnostic. The second goal is particularly important for identifying the contribution of Ge/Zr filter layers to diffraction data for physics packages using those materials.

This campaign used a single day on EP, with two shot designs for each material: one for ramp compression to 1.2Mbar, and another for ramp compression to 2.4Mbar. This comprised 4 unique target material/drive configurations, which were duplicated to mitigate risk of a missed measurement. The drive designs consisted of 2 stitched pulse shapes (2 sequential beams) to define a 20ns ramp, while the Ge backlighters were driven using the same pulse shape on each of the remaining 2 beams. The physics packages consisted of Beryllium ablators, 20μm of Ge or Zr, and a LiF windows mounted to W pinholes on the PXRDP diagnostic. Germanium backlighters were used to generate ~1ns duration X-ray pulses to interrogate the target material at the predicted peak pressure state. Velocimetry of the LiF/Ge (or Zr) interface was measured via ASBO for comparison to simulations. Lastly, the X-ray spectrometer, pinhole cameras, and SPC were fielded to assess backlighter performance.

Excellent ASBO measurements delivered high-fidelity velocimetry for each material/pressure configuration, which demonstrated good agreement with post-shot simulations (see Figure). This suggests adequate fidelity in the EOS's used for Ge and Zr over these pressure ranges. Issues with backlighter performance, however, led to a loss of PXRDIP data for both shots studying Ge at 1.2Mbar. The 2.4 Mbar Ge data indicated fairly weak scattering from a non-cubic solid phase. The diffraction data for the Zr shots also show diffraction from solid, non-cubic phases, but with strong preferred orientation. Analysis of these results is ongoing, with the goal of producing a peer-reviewed publication. The results of this campaign – specifically the positions of strong Bragg lines – will be used to help interpret diffraction data for targets using Ge and/or Zr filter layers in the future.

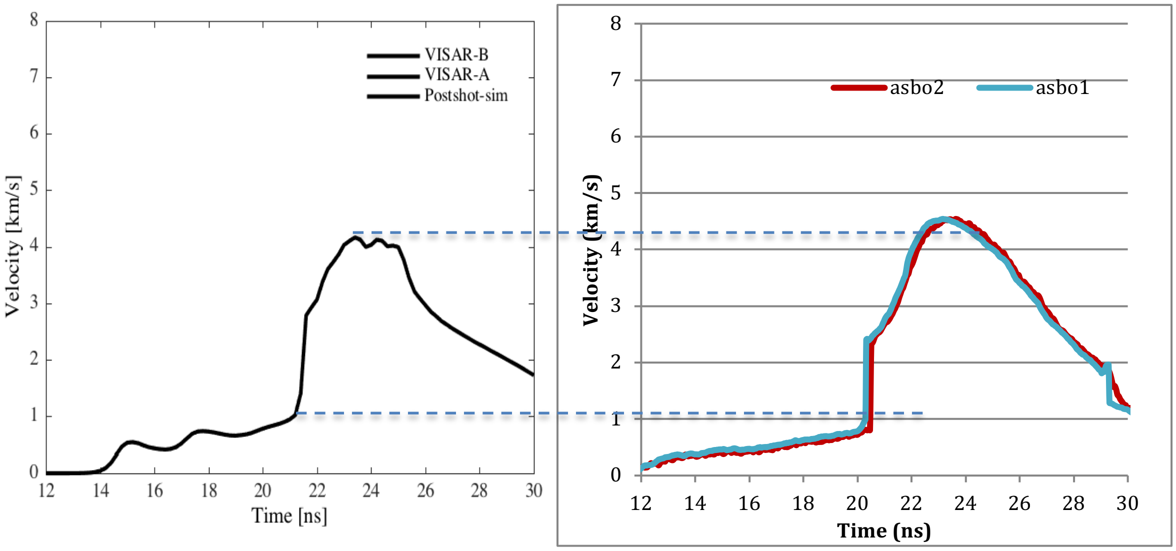

Figure 1 – Velocimetry results for 1.2Mbar Ge. The Ge/LiF interface velocity from post-shot simulation (left) shows good agreement with ASBO measurements (right)

3. Development of Time-Resolved X-Ray Diffraction Techniques (PI: L. R. Benedetti)

with F. Coppari, J. R. Rygg, A. E. Jenei, J. Eggert, G. Collins, D. K. Bradley, J. Kilkenny

Two FY18 shot days on Omega-EP were used for development of a capability to measure x-ray diffraction of compressed materials at multiple times during a single-laser experiment. The experimental design is based on the PXRDIP platform that has already been successfully used to measure x-ray diffraction of compressed materials onto image plates. The idea of this campaign was to adapt the PXRDIP platform to allow access to an x-ray streak camera to measure a continuous record of x-ray diffraction in addition to the image plate measurement (see Figure).

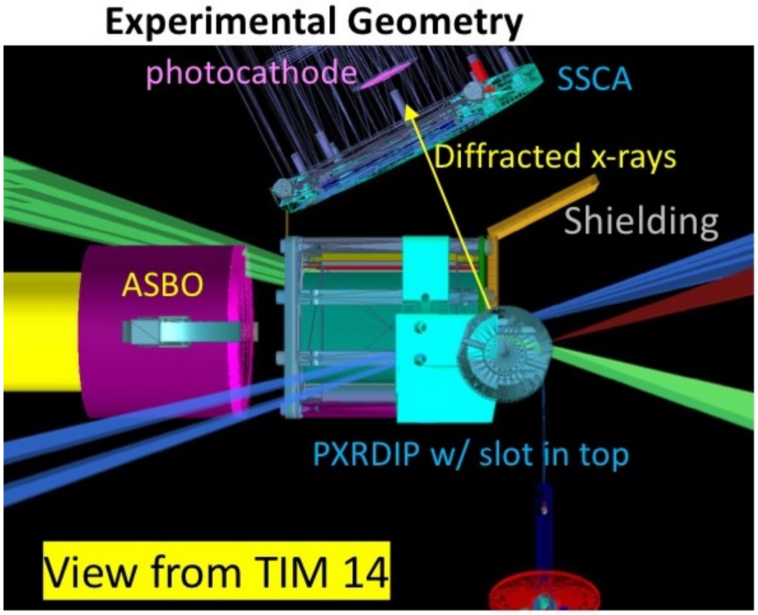

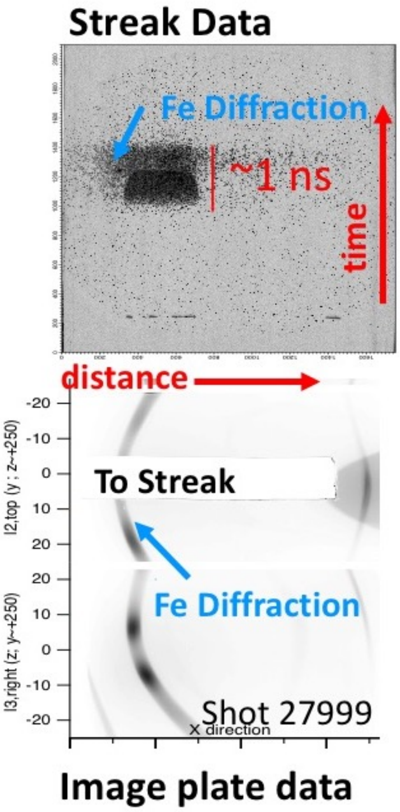

Left. Experimental geometry showing close approach of x-ray streak camera to PXRDIP. **Right**. X-ray diffraction of uncompressed iron streaked on film (**top**) and integrated on image plate (**bottom**).

The entire series of shots used an iron target and a laser pulse designed to drive the iron through the alpha-epsilon phase transition. The first shot day confirmed the pressure history and phase transformation with VISAR and image plate data. However, no coherent data was found on the x-ray streak camera. The second shot day reduced electronic noise to the streak camera by moving it from TIM14 to TIM10, and substantially reduced x-ray backgrounds by adding additional shielding. With these changes and also an enlarged target, the first streaked x-ray diffraction was seen, for an undriven (uncompressed) target (top right in Figure). Streak diffraction has not yet been observed a compressed target, and the data suggests that the streak camera gain mechanism is substantially upset by the interaction of the drive laser pulse with the PXRDIP target. An upcoming campaign in FY19 is planned, to address the electromagnetic upset of the streak camera by replacing the PXRDIP with a smaller target geometry, and to explore the use of imaging diagnostics to complement the streaked diffraction data.

4. Development of an In-Situ Pressure Standard for Diffraction Experiments (PI: F. Coppari)

With: J. Eggert, R. Kraus

The goal of this campaign is to develop a new way of determining pressure in diffraction experiments based on the use of an in-situ pressure gauge. By measuring the diffraction signal of a standard material (whose equation of state is known) compressed together with the sample, one can determine the pressure upon ramp-compression.

Currently pressure is determined from VISAR measurements of diamond free surface velocity or particle velocity through a transparent window (such as LiF or MgO). This method is in some cases ambiguous (lack of reflectivity or shock formation) or relies on assumptions and equation of state models. Cross-checking the VISAR measurement with in-situ pressure determination using the diffraction signal of a standard material will improve the diffraction platform by providing a complementary way of determining the pressure state within the sample, with great impact to the broader effort of determining structures and phase transitions at high pressure and temperature. In addition, combining pressure determination from VISAR and from the in-situ gauge can give information about the temperature of the sample by measuring the calibrant thermal expansion.

Building upon the results obtained in previous campaigns that focus on diamond windows and ramp compression at 200 GPa, the goals for the half-day campaign in FY18 were to push to higher pressure and to extend the study to other window materials, such as MgO and LiF. Half of the shots looked at the diffraction patterns of the Au/Ta and Pt/W pairs coated on diamond windows (Fig.1a) and ramp compressed to 400 GPa. The other half were ramp compression experiments to 200 GPa using MgO windows. All shots gave good quality data (Fig.1b) and analysis is being finalized. Comparison of the pressures obtained from VISAR analysis and from the diffraction patterns provide information regarding the accuracy of the VISAR method as well as the possible existence of pre-heating.

Future directions of this work will look at characterizing the pressure standards at higher pressure and implementing this technique into a real diffraction experiment. Although this platform still needs some development effort before it can be routinely used in diffraction experiments, the data collected so far are extremely encouraging and suggest that the use of an in-situ pressure gauge can be a viable path forward in future x-ray diffraction measurements both at Omega and NIF.

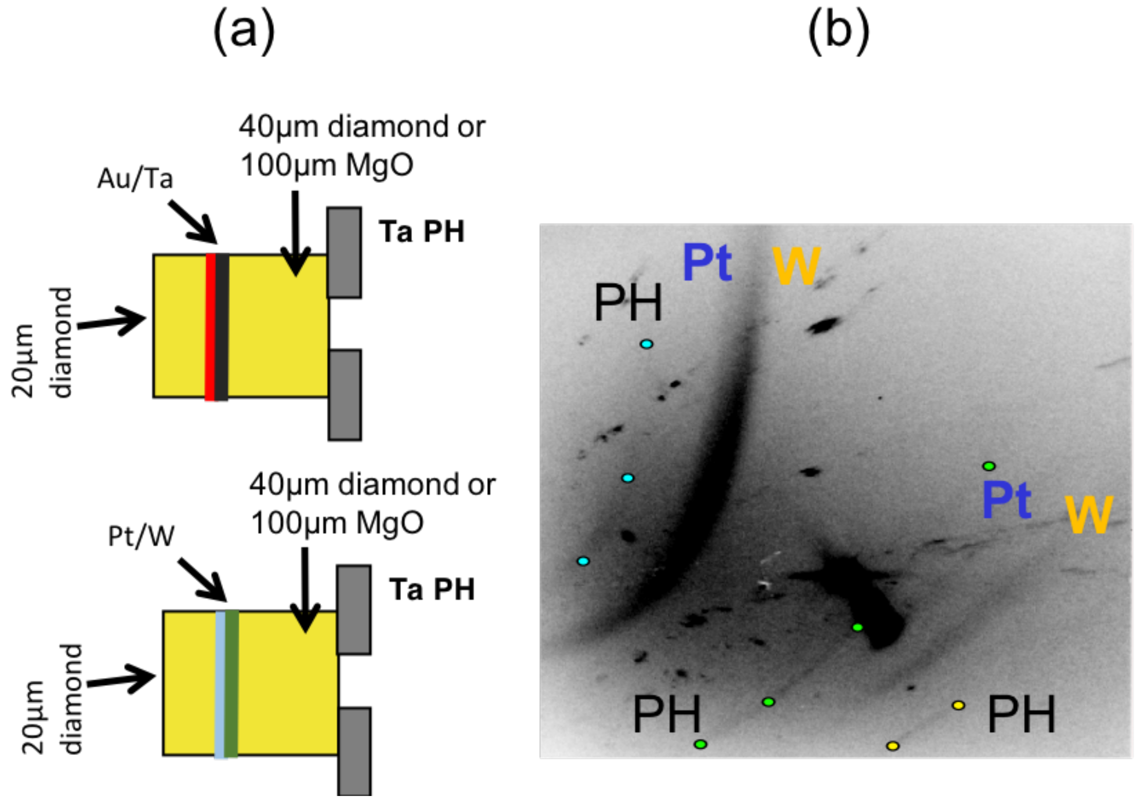

Figure 1: (a) Schematic of the target assembly. Diamond or MgO windows were coated with 1 µm thick Au/Ta or Pt/W pairs used as pressure standards in the diffraction experiment. All targets had 20 µm diamond ablator and were mounted on Ta pinholes. (b) Representative raw diffraction data. The dots overlap with the diffraction signal from the Ta pinhole, while labels point to the signals from compressed Pt and W. At least two diffraction lines are observed for each standard.

B. Material Equation of State Using Other Techniques

1. Development of a Platform for Equation of State Measurements Using Mo Flyer Plate Impact (PI: F. Coppari)

With: R. London, P. Celliers, M. Millot, D. Fratanduono, A. Lazicki, and J. Eggert

This campaign is developing a platform to use the Omega laser to accelerate flyer plates to hyper-velocity for absolute equation of state measurements by symmetric impacts. The concept is to use ramp compression to accelerate a Molybdenum (Mo) foil across a vacuum gap through indirect laser ablation, and observe the flyer impact on a same-material sample mounted side-by-side with a transparent Quartz window (see Fig. 1). By measuring the flyer-plate velocity prior to impact through the transparent window, and the resulting shock velocity in the Mo sample using transit time measurements, the principal Hugoniot of Mo can be determined *absolutely* (e.g. without needing a known pressure reference), enabling the development of an EOS standard. This platform will be valuable all activities interested in equation of state and Hugoniot measurements at pressures higher than 12 Mbar, where currently there are no materials whose EOS has been experimentally determined.

The FY18 shots built upon the results obtained in FY17. Target design was improved by changing window material from LiF to Quartz. This allows both a better measurement of the flyer velocity prior to the impact, and also enables shock velocity to be measured in the Quartz after the impact, therefore being able to cross check the shock state obtained in the Mo. The first half-day explored the Hugoniot of Mo up to shock speeds of 18 km/s. The second half-day pushed to higher velocities (hence higher pressure) and filled in dataset gaps at lower velocity, to be able to better compare these results with different measurements and validate the platform.

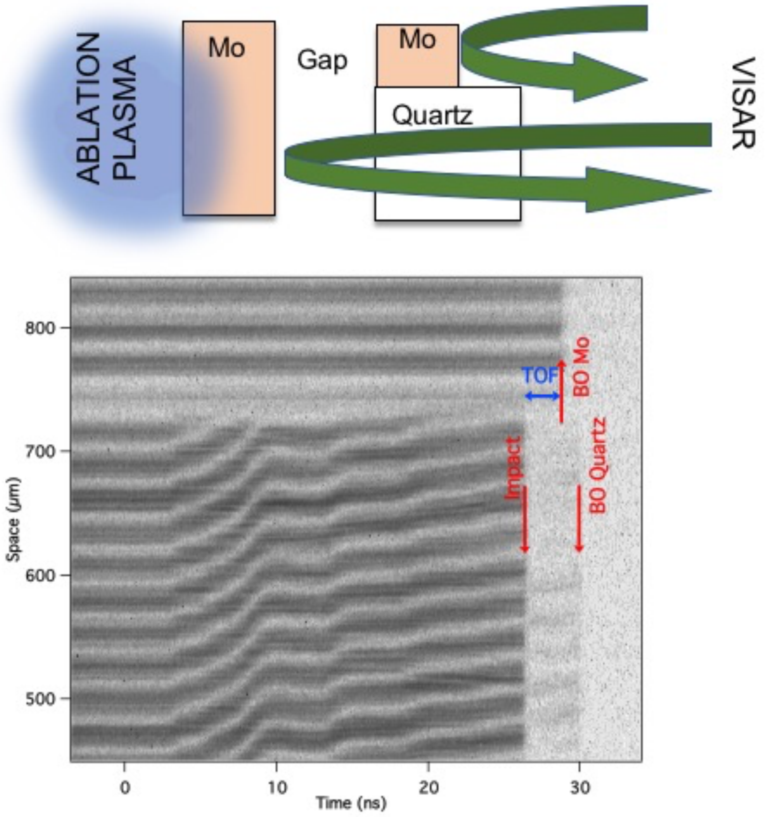

Figure 1:
(Top) Schematic of the experimental setup. A Mo foil is accelerated across a vacuum gap and impacted on a transparent Quartz window, side-by-side with a Mo foil. Simultaneous VISAR measurements of the flyer velocity and shock velocity upon impact give a measurement of the Mo EOS, without the need to rely on the EOS of a reference material.

(Bottom) Representative VISAR record. The main events are indicated by arrows.

2. Development of a Platform for Absolute Equation of State Measurements Using Diamond Flyer Plate Impacts (PI: F. Coppari)

With: R. London, P. Celliers, M. Millot, D. Fratanduono, A. Lazicki, and J. Eggert

This campaign develops a platform to accelerate diamond flyer plates to hyper-velocity for absolute (i.e reference-free) equation of state (EOS) measurements. Ramp compression of diamond through direct laser ablation results in a slow acceleration of the diamond across a vacuum gap. After propagating a known distance, the diamond flyer impacts on a transparent diamond window. By measuring the diamond flyer-plate velocity prior to impact and the resulting shock velocity in the diamond witness, the principal Hugoniot of diamond can be determined *absolutely* (e.g. without needing a known pressure reference), enabling the development of diamond as an EOS standard. Figure 1 illustrates the approach and sample data. Note that this campaign is relevant to all activities interested in equation of state and Hugoniot measurements at pressures higher than 12 Mbar, where currently there are no materials whose EOS has been experimentally determined.

The specific goal of the FY18 half-day was to fill in gaps in the data set and push to higher pressure. With 8 successful shots, the diamond Hugoniot EOS has been characterized up to about 30 km/s (corresponding to 15 Mbar). Experience gained in past campaigns led to improvements in target design resulting in extremely high-quality data. Data analysis now underway is expected to result in an accurate equation of state for diamond measured without relying on the EOS of reference materials.

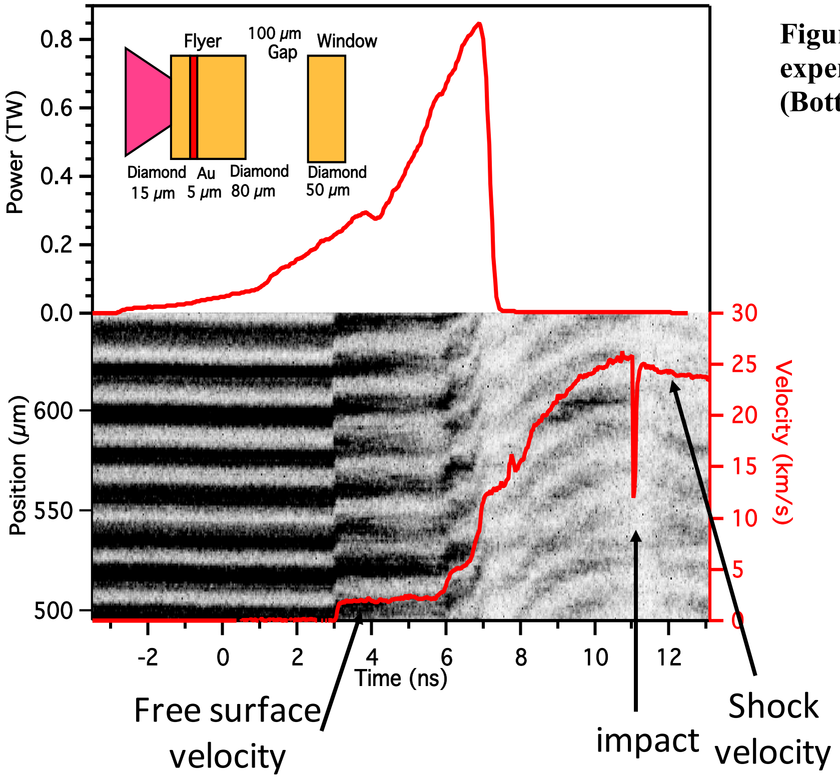

Figure 1. (Top) Diamond-Flyer experimental configuration. (Bottom) Sample VISAR data

3. Equation of State Measurements from CH Foam in a Spherically Convergent Geometry (PI: A. M. Saunders)

with A. Jenei, T. Doeppner, M. J. MacDonald, D. Swift, H. Whitley, J. Nilsen

This experimental campaign aimed to develop a technique to make off-Hugoniot equation of state (EOS) measurements in CH by compressing half-density CH foam in a spherically convergent geometry. The lower starting density allows the spheres to reach higher temperatures as the shock coalesces, which can provide equation of state measurements at pressures exceeding 100 Mbar. There is currently a dearth of experimental data to benchmark EOS models at such extreme conditions. In addition, the campaign sought to establish a new technique to measure temperature within the shock front: x-ray fluorescence spectroscopy.

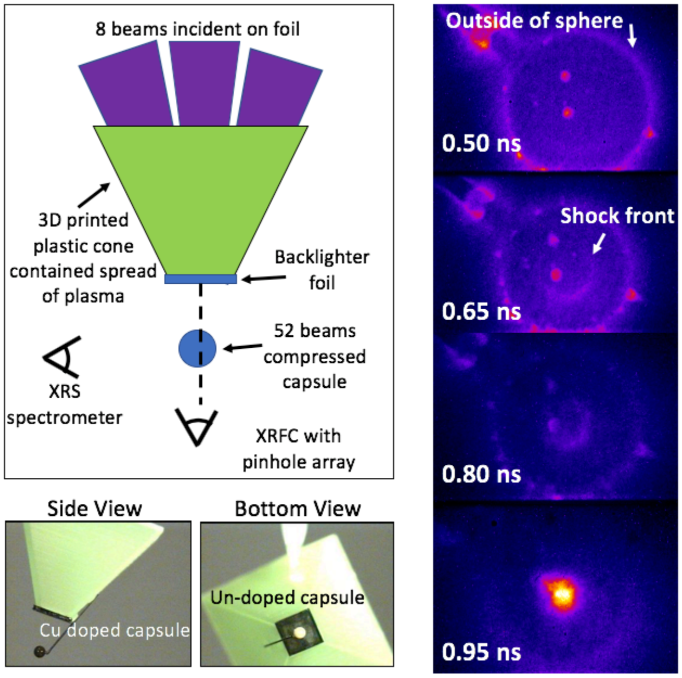

Figure 1. Experimental configuration, target photos, and x-ray framing camera data from shot 88630.

The upper left of Figure 1 shows a schematic of the experimental configuration. 52 laser beams directly drive a foam capsule for 1 ns. As the sphere compresses, 8 laser beams heat a foil suspended at the bottom of a plastic cone to generate a He-α x-ray backlighter; the plastic cone contains the spread of plasma. An x-ray framing camera (XRFC) with a pinhole array takes backlit 2-D time-gated images of the capsule as it implodes and the XRS spectrometer measures the emission spectrum from the backlighter foil and the capsules. The half-density CH foam capsules are 500 microns in diameter with 20 μm thick ablator layers of GDP plastic. This is the first time such capsules were used, and required significant R&D from their creator, General Atomics. Several of the foam spheres are doped with 1 at.% Cu; this doping process is also new, and dopant concentrations were uneven inside the spheres. Pictures of the assembled targets from the OMEGA shot day can be seen in the bottom left of Figure 1. The backlighter foil is vanadium for the un-doped capsules and germanium for the Cu-doped capsules.

The FY18 shots acquired high quality data from the Cu-doped capsules, but the vanadium He-α backlighter proved too high in energy to resolve the shock front in the capsules without a dopant. The right side of Figure 1 shows four framing camera images from a Cu-doped capsule. The shock front is seen progressing towards the center until shock coalescence, around 1 ns. XRF data was also collected for the Cu-doped spheres and will be compared with simulations in order to benchmark the temperatures of the samples. Analysis of the data is ongoing. In addition, the foam capsules developed as a result of this campaign were subsequently used in a NIF discovery science shot day. Future campaigns will improve upon the platform to provide benchmarking EOS measurements of materials at extreme conditions.

4. Developing a Conically-Convergent Platform for Measuring Hugoiot Equation of State in the 100 Mbar-Gbar Pressure Regime (PI: A.E. Lazicki)

with M. C. Marshall, D. Swift, F. Coppari, R. London, D. Erskine, H. Whitley, and J. Nilsen

This campaign continued to develop a platform for measuring Hugoniot equation of state (EOS) of arbitrary (including high-Z) materials at pressures much higher than can be achieved using a standard planar drive. This platform is intended to collect data in the 100+ Mbar pressure regime, where currently very little data exist for any material, for the purpose of constraining equation of state models.

To achieve the desired pressure amplification, converging shock waves are launched into a plastic cone inset in a halfraum. For appropriate cone angles, nonlinear reflections of the shock wave result in formation of a Mach stem: a planar high-pressure shock that propagates along the axis of the cone.

This new platform was tested on one half-day in FY16 and one half-day in FY17, showing that a high-pressure Mach stem formed, but was not supported through the full thickness of the cone and impedance-matching physics package, primarily because of the pulse length limitations for the highest energy drives; a release wave rapidly degrades the Mach wave after the 1-ns drive turns off. The 2 half-day campaigns in FY18 tested a reduced-scale hohlraum and cone, longer pulse lengths, and a low pressure gas fill, to support the Mach stem long enough to perform an EOS measurement. The campaigns also experimented with various thicknesses of Au heat shielding in the targets, as well as bromine-doping of the Mach cones to mitigate preheat.

In the FY18 shots, the small hohlraums easily generated 100 Mbar states in the targets (Figure 1a), but also generated sufficient hard x-rays to cause the target surfaces to quickly lose reflectivity, even when thick (25 micron) Au heat shields were employed. In the absence of reflected VISAR light, shock wave breakouts were registered using the thermal signature in the streaked optical pyrometer. Longer pulse lengths effectively delayed the release waves (Figure 1b), but the surface area of the Mach wave is too small at this reduced scale to make a high-accuracy EOS measurement with the current VISAR optics. Inclusion of a gas had no consistent observable effect on the Mach wave propagation. The second half-day added diagnostics to collect data on hard x-ray and hot-electron production, which are being analyzed to understand how to mitigate the preheat. Future shots will increase the hohlraum scale and the length of the drives, and will experiment with techniques for quantifying the preheat.

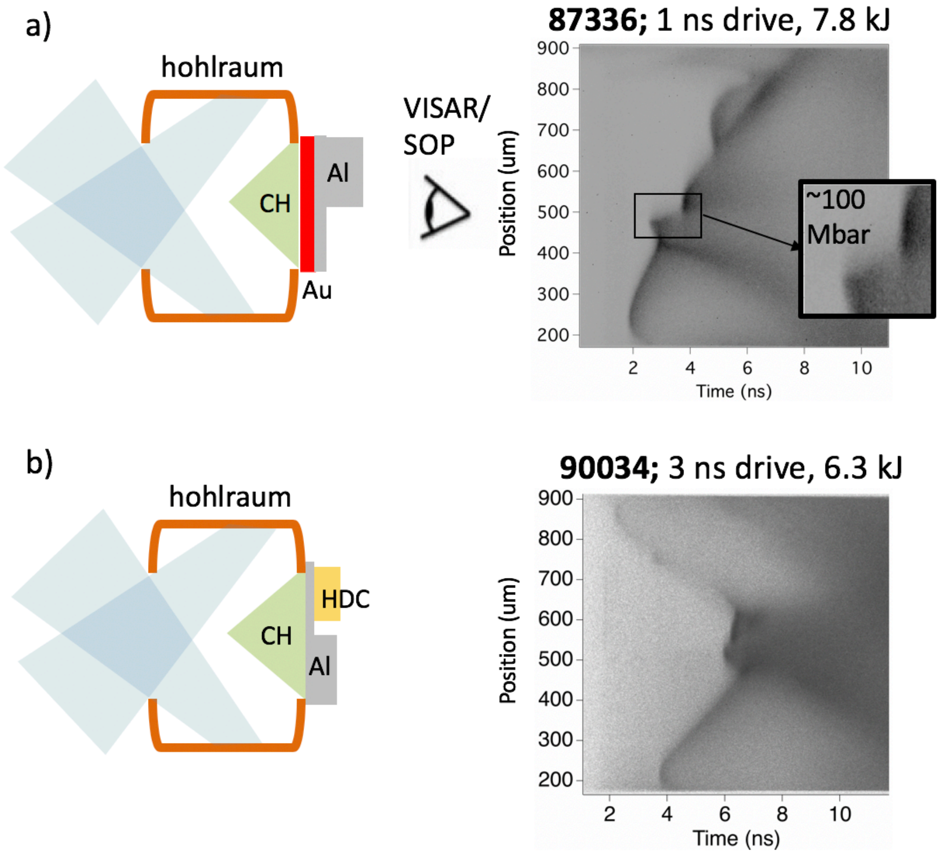

Figure 1. Target configuration and shock wave breakout measured with the steaked optical pyrometer (SOP) for two FY18 shots. (a) Shows the effect release waves degrading the central quasi-planar region of the driver. The breakout times from 20 um and 100 um Al steps indicate a shock velocity corresponding to ~100 Mbar in Al. (b) Shows data obtained with a longer (3 ns) drive and lower energy, effectively delaying the release waves. However, the planar region of the Mach drive is too small to encompass both Al and HDC steps and the Al base in the impedance-matching target.

5. Experiments to Test the Effect on Target Reflectivity of Release Across a Phase Boundary (PI: R.F. Smith, LLNL)

with A. Fernandez Pañella, D. Fratanduono, and J. Wicks (Johns Hopkins University)

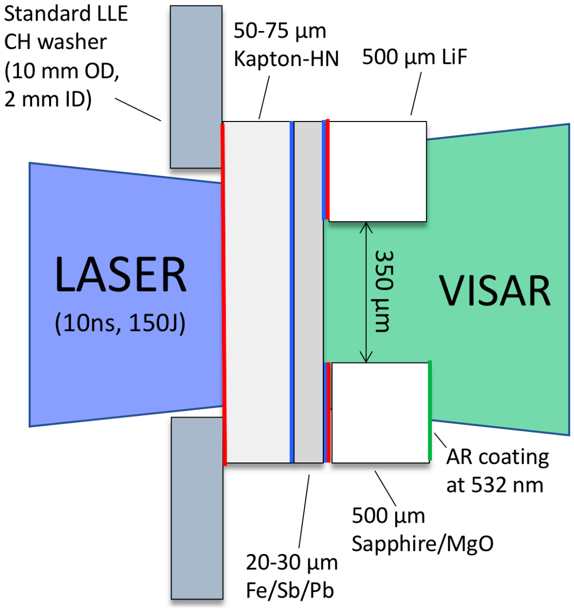

Figure 1. Target design for Phase Transformation Release on Omega-EP. Under steady-shock conditions VISAR measures the sample free-surface velocity and sample window particle velocity.

The goal for the PhaseTransRelEP-18A (Dec. 6th) campaign was to determine how pressure release across a phase boundary affects target reflectivity. These experiments were in support of ramp equation-of-state experiments conducted on the NIF [1]. The target design for these experiments is shown in Fig. 1 and consists of a 50-75-μm CH ablator, a 20-30-μm layer of either Pb, Sn or Fe, and over the 1-mm VISAR field of view a free-surface region, a region with a LiF window and a region with an MgO/sapphire window. These experiments used the 10-ns ERM99v016 pulse shape to drive a temporally steady shock into the target assembly. Sample free-surface velocity (u_{fs}), particle velocity (u_p) and reflectivity were monitored with the line-VISAR (ASBO) system. Drive beam energies were varied from 67 to 755-J to generate different initial pressure states along the shock-Hugoniot.

In this experiment, shock compression is followed by isentropic pressure release. Depending on the initial shock compression state, isentropic pressure release may cause the material to decompression across a solid-solid phase boundary or a solid-liquid phase boundary. These experiments measured the correlation between free-surface target reflectivity with release from different shock states, and found that while the free-surface reflectivity was virtually unperturbed by isentropic release across solid-solid phase boundaries, it dropped precipitously for pressure release paths across solid-liquid phase boundaries.

In addition, this data allows a test of the commonly used approximation of $u_{fs} = 2 \times u_p$. Some preliminary VISAR data is shown in Fig. 2. Figure 2a shows the VISAR fringe movement from the Fe/sapphire and Fe free-surface velocity interfaces. The associated extracted velocity profiles are shown in Fig. 2b (red traces). Predicted outputs from a HYADES 1D hydrocode simulations are shown as black dashed traces. Velocity structure on the way to peak velocity is due to changes in material sound speed associated with the alpha-epsilon phase transformation.

[1] R. Smith, *et al.*, Equation of state of iron under core conditions of large rocky exoplanets. *Nature Astronomy* 2, 452–458 (2018).

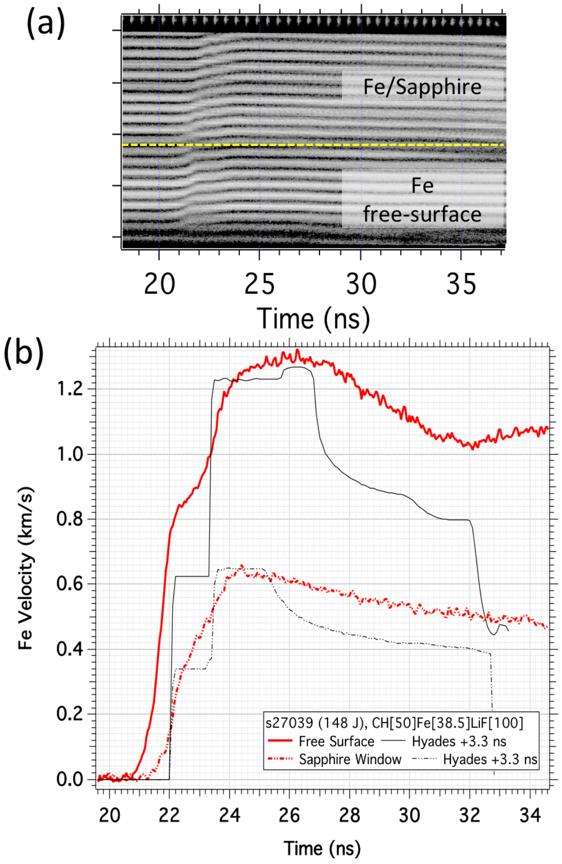

Figure 2. (a) Raw VISAR data showing regions of Fe/Sapphire and Fe free-surface. (b) Extracted velocity profiles and simulations from the Hyades hydrocode.

6. Liquid – Ice VII Phase Transition Kinetics in Ramp Compressed Water (PI: M. C. Marshall)

with D. E. Fratanduono, M. Millot, and R. F. Smith

The goal of the FY18 RampWater shot series was to observe the liquid–ice VII phase transition in water ramp compressed along its principal isentrope at ultrahigh strain rates (>10^6 s^{-1}). The isentrope crosses the phase boundary at ~2.5 GPa; however, ramp-compression experiments at the Sandia Z machine showed an over pressurization of the phase transition at 7 GPa [1]. An LLNL kinetics algorithm predicts freezing at ~9 GPa for the OMEGA experiments, which have ~10x higher strain rates than the Z experiments.

Two half day campaigns were performed at the OMEGA facility. Water was ramp compressed using a release reservoir design in which shocked CH releases across a vacuum gap and isentropically loads the water cell, as shown in Figure 1. A thin water layer (~20 μm), created using a sapphire "diving board" configuration inside the water cell, was ramp compressed to ~15 GPa. The experiments were designed to observe two signatures of the phase transition using VISAR. The first is a stress release on the rear sapphire window of the thin water layer caused by volume collapse during the transition (ice VII is 60% more dense than liquid water). The second is a coincident dip in transmission through the water layer from optical scattering of the coexisting liquid and ice phases with different refractive indices.

Preliminary analysis indicates possible stress release signatures near the predicted pressure of 9 GPa in several shots, but no clear evidence for transient opacity has been identified so far. Analysis is ongoing to discern the stress release on the water/Al/sapphire interface (lower region in Figure 1) and a follow-up campaign is scheduled at Omega EP in FY19.

[1] D. H. Dolan, M. D. Knudson, C. A. Hall, and C. Deeny, Nat. Phys. 3, 339-342 (2007).

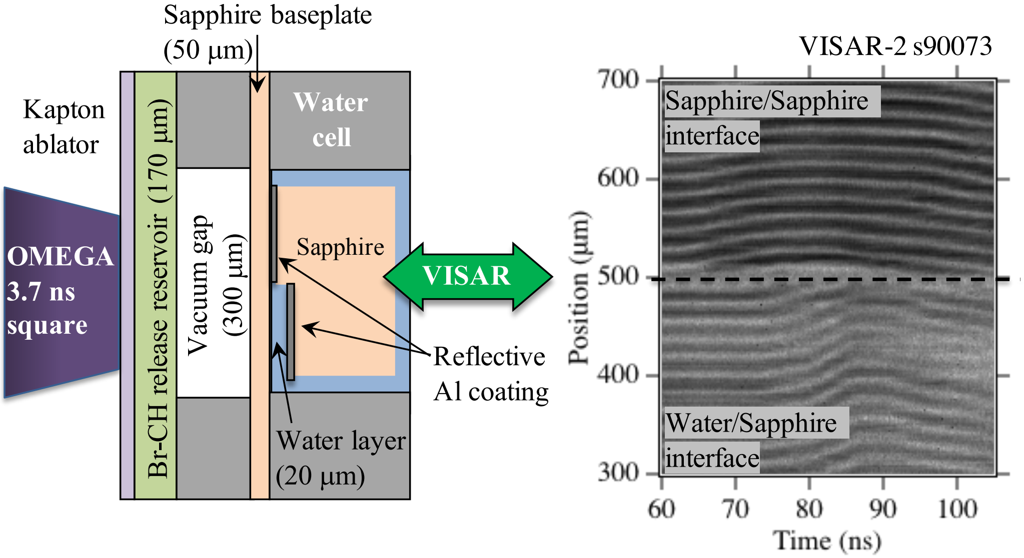

Figure 1. (Left) Target design for a stress release measurement. (Right) corresponding VISAR image showing interface motion of the two Al-coated surfaces inside the water cell. The velocity of the sapphire/Al/sapphire interface (upper region in water cell and VISAR data) provided a drive measurement for each target shot.

7. First Measurements of the Single-Crystal TATB Hugoniot to 80 GPa (P.I.: M. C. Marshall)

with A. Fernandez Panella, T. Myers, J. H. Eggert, T. Bunt, L. Lauderbach, L. D. Leininger

The purpose of the HEEOSEP-18A campaign was to measure the Hugoniot of TATB (triamino-trinitrobenzene) shocked to high pressure. TATB is a high explosive known for its insensitivity to high temperatures and impacts. Experiments were done at the Omega EP laser facility, where TATB was shocked to a range of pressures (15 – 80 GPa) over 8 shots. Hugoniot data were obtained by impedance matching relative to an aluminum standard. Planar targets had a Kapton ablator, aluminum base plate (standard), single-crystal TATB sample, and LIF witness used to correct for shock unsteadiness. Three laser beams with total energies of 580-2300 J were stacked in time, producing a 30-ns drive to support a nearly steady shock in the TATB. VISAR was used to measure interface velocities and shock transit times needed for the impedance-match analysis. The results will be used to improve predictive modeling for TATB.

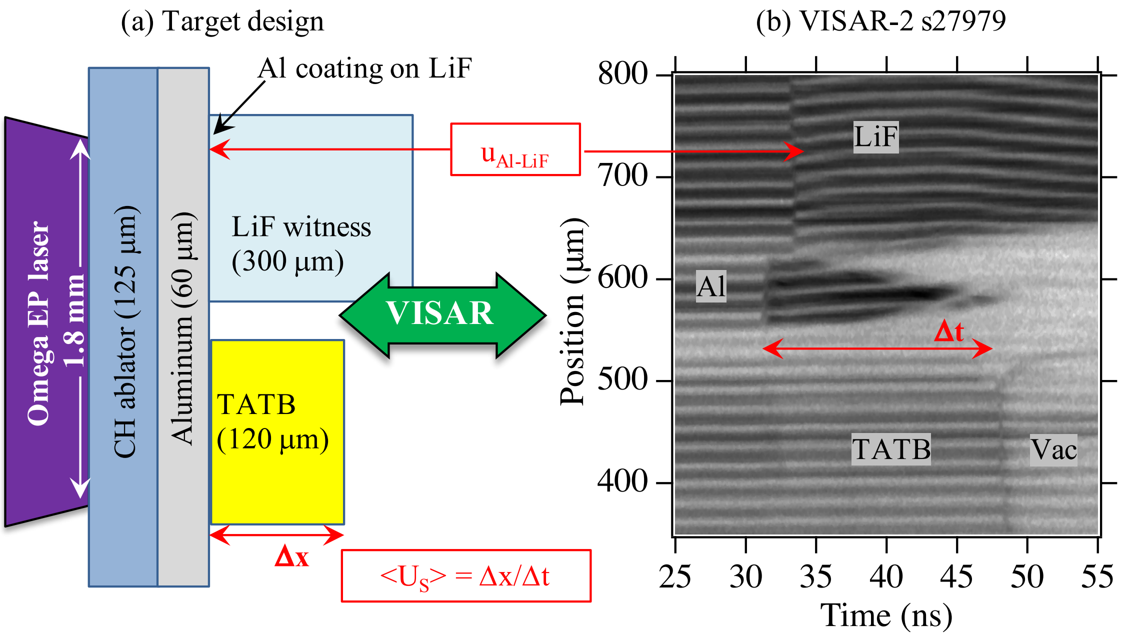
(a) Target design

(b) VISAR-2 s27979

Figure 1. (a) TATB target design and (b) VISAR data showing the shock transit time (Δt) in TATB, and the Al/LiF interface velocity.

C. Material Dynamics and Strength

1. Rayleigh-Taylor Growth in Ramp-Compressed Copper (PI: J.M. McNaney)

with S. Prisbrey, A. Krygier and H.-S. Park

The CuRT-EP-18A series of shots investigated inconsistencies in the liquid copper Raleigh-Taylor data from previous FY17 campaigns. The previous campaigns indicate that the simulated growth behavior is not capable of matching the liquid RT growth throughout the entire loading history (figure 1). As RT growth is driven by acceleration of the ripples into a lower density medium, it appears the acceleration history in the simulations was not sufficiently representing the driving force actually seen in the experiment.

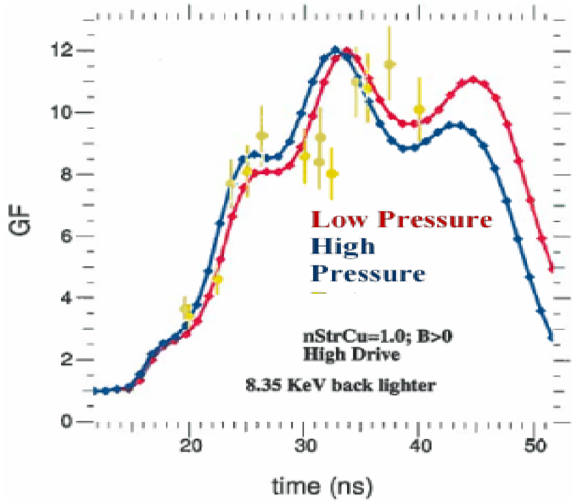

Figure 1. Comparison of simulations (solid lines from bounding cases) and experiments (yellow points from CuRT-EP-17A and B).

Considerable experimental and simulation sensitivity analysis led to a hypothesis that reverberations interact with the incoming drive plasma column and lead to complicated shock-release-reshock paths that are not well represented by the existing equations of state.

The FY18 campaign made use of drive analog targets and the ASBO diagnostic to measure the magnitude and timing of reverberation features expected from the simulations, to assess the sensitivity of the experiment to various EOS assumptions. Multiple target designs were used to mitigate risk associated with uncertainties in the behavior of target materials under shock loading.

The primary result of the single day of experiments is shown in Figure 2. The expectation was for a reverberation to appear at about 25ns; this reverberation is associated with the RT growth that occurs at about 30ns in the simulations shown in Figure 1. The actual reverberation appears about 3-4ns later and is somewhat smaller than expected. Other shots confirmed this observation and provided additional observations that will help in characterizing dependency on sample dimensions and drive strength.

Based on this observation we believe we understand the origin of the disagreement between experimentally measured and simulated RT growth in liquid copper. Future work will incorporate these results into modeling of the RT growth and re-assess the ability of the simulations to accurately represent the observed growth.

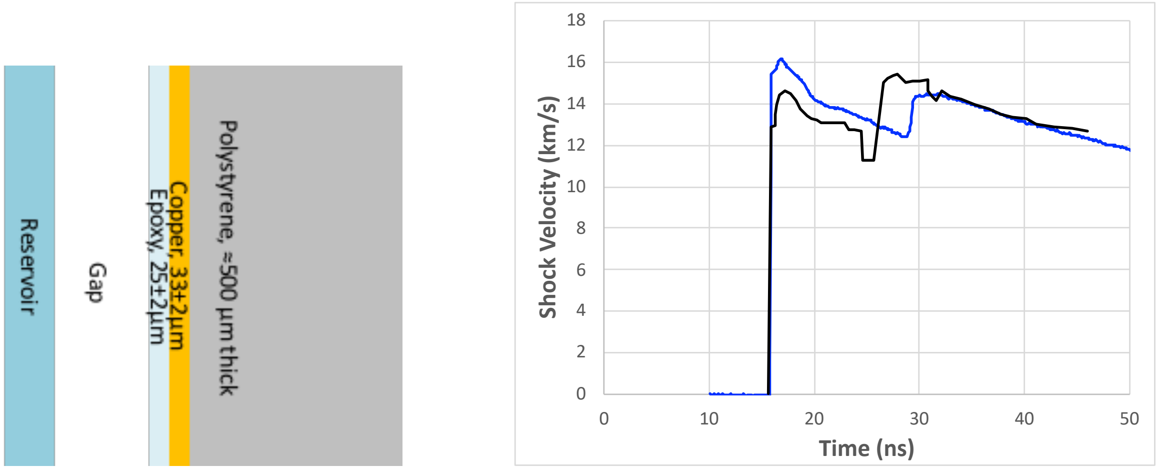

(a) (b)

Figure 2. (a) Target used for shot S28641. (b) Comparison of pre-shot simulated (solid black line) and experimental (blue line) shock velocity. The measured reverberation arrives about 3ns later than simulated.

2. Development of Pressure-Time Pulse Shaping in Ramp Compression Experiments Using Graded Density Additively-Manufactured Foams (PI: R. Smith)

with Suzanne Ali, James Oakdale, Juergen Biener, H.-S. Park, S. Prisbrey, P. Amendt

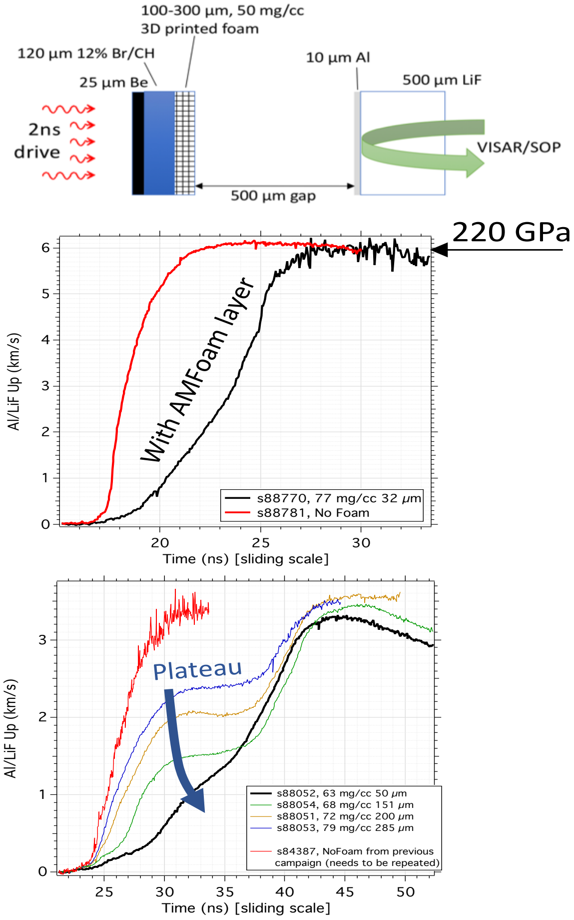

Figure 1. (Top) Target design for AM Foam shots. (Middle) When ramp compressing to 220 GPa peak pressure the rise time of the ramp compression wave increases significantly due to the inclusion of the AM Foam layer. (Bottom) The thickness of the AM Foam layer determines the pressure (velocity) extent of the plateau in the compression profile.

In support of Material Strength experiments on the National Ignition Facility,
the goal of these experiments is to shape the pressure profile in a piston driven ramp-compression platform [1] by incorporating an additive manufactured foam layer (AM Foam) into the sample design (see Fig. 1, top). The 3D printed foams are characterized as follows [2]: The 100×100×16 μm^3 log pile blocks composed of individually printed lines, are stitched together to form layers that are 1.7 mm^2 in diameter. Seven 16 μm^3 layers are then stacked on top of one another to arrive at cylindrical "AM foams" that are 1.7 mm^2 in diameter and 112 μm tall [2]. These foams are glued onto a 25 μm Br + 120 μm 12% Br/CH assembly (Fig. 1, top). For some shots the overall thickness was varied. Following the prior ramp compression design [1], fifteen beams of the Omega laser with 300 J in 2 ns launch a ramp compression wave being into an Al/LiF sample (Fig. 1, top). Throughout these campaigns, different shots have varied the thickness and density of the 3D printed foam with the goal of optimizing the temporal ramp profile. Changing the laser energy causes the pressure in the Al sample to vary. In the example velocity profiles in Fig. 1 (middle), as determined by VISAR, the rise time of the compression wave increases several fold due to the inclusion of the AM Foam layer. Further modification of the compression wave pulse shape is possible by varying the thickness of the AM Foam layer (Fig. 1(bottom)). Here, a velocity plateau is evident but diminishes with decreasing AM Foam thickness.

[1] R.F. Smith et al., "High planarity x-ray drive for ultrafast shockless-compression experiments" Phys. Plas. **14**, 057105 (2007).

[2] James S. Oakdale, Raymond F. Smith, et al., "Direct Laser Writing of Low-Density Interdigitated Foams for Plasma Drive Shaping", Adv. Funct. Mater. 1702425, (2017); DOI: 10.1002/adfm.201702425

3. Rayleigh-Taylor Growth Measurements in Depleted Uranium (PI Team: J.M. McNaney, Ray Smith and H-S. Park)

This campaign is to develop a new ramp drive by laser-pulse shaping that can maintain the depleted uranium (DU) sample in solid state while driving to 1-2 Mbar peak pressure. If successful, this drive will be used to measure DU strength by measuring the ripple growth amount from Rayleigh-Taylor instability. A 30 ns-long pulse shape was designed by stitching 3 10 ns-long beams, as shown in Figure 1 (a), and the drive is measured with the VISAR diagnostic. The VISAR targets consist of an ablator (Be), a witness plate (Ta or Cu) and a LiF window. The first campaign used a variety of targets with different styles of witness samples. The VISAR produced meaningful data as shown in Figure 1 (b) and (c). The raw fringe traces are shown in (b) and the analysis of this shot is shown in (c). Also shown is the 1D Hyades simulation. The agreement is remarkable except for a small amount of timing shift. However, during the first of two shot days in FY18, the shot-to-shot repeatability was not very good, mainly due to non-uniform glue thicknesses and a non-planar target component. The second day attempted to fix this issue. Glue usage was removed by depositing rather than adhering the Cu witness sample, and planarity was improved by polishing the target component. The repeatability was greatly improved, and the campaign returned data to understand the effect of composite pulse shaping through beam "stitching". The next step is to apply this drive on rippled targets and measure growth factors.

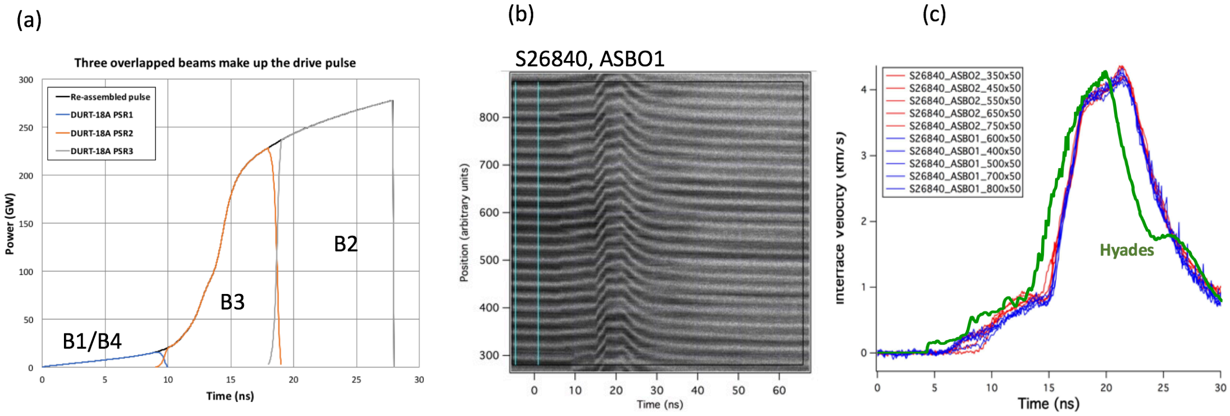

Figure 1. (a) Three-beam "stitched" pulse shape to create a directly driven ramp drive for the strength campaign; (b) Raw VISAR data using the designed pulse shape; (c) Analyzed VISAR data and comparison with a 1D Hyades simulation.

4. Modulation Transfer Function Accuracy for Rayleigh-Taylor Growth Experiments (PI: E. Gumbrell)

with H-S Park, C. Huntington, A. Krygier and J.M. McNaney

This campaign aimed to quantify and reduce the systematic error induced by uncertainties in the modulation transfer function (MTF) used to analyze ripple growth for the material strength campaign. The MTF is a measure of spatial resolution in an optical imaging system and mathematically is the Fourier transformation of the line-spread function. The strength campaign radiographs the ripple growth and corrects for the MTF as measured by an X-ray knife-edge included with the target. The uncertainty of this method arises mainly from uncertainty in the spatial profile of the X-ray backlighter, that very often consists of 2 sources – one sharp spot that achieves high resolution, and a second, broader spot from the transmission of high-energy x-rays through the thin section of the collimator. This campaign obtained data on the MTF using large amplitude undriven ripples in a single shot. The systematic error was determined by comparing the analyses between the ripple amplitude measurement using the steps and the MTF, and the known ripple amplitudes from the target metrology. High quality radiography images were obtained as shown in Figure 1 (a) from this campaign. The analysis of the MTF from this image is shown in Figure 1 (b), including both the high-resolution source (green line), the lower-resolution source (orange line) and the combined system MTF derived from the convolution of these sources (blue line). Using this MTF and comparing with the known ripple amplitudes leads to a conclusion that the systematic error of the ripple growth factor analysis is less than 10%. The results of this campaign were published in Review of Scientific Instruments [1].

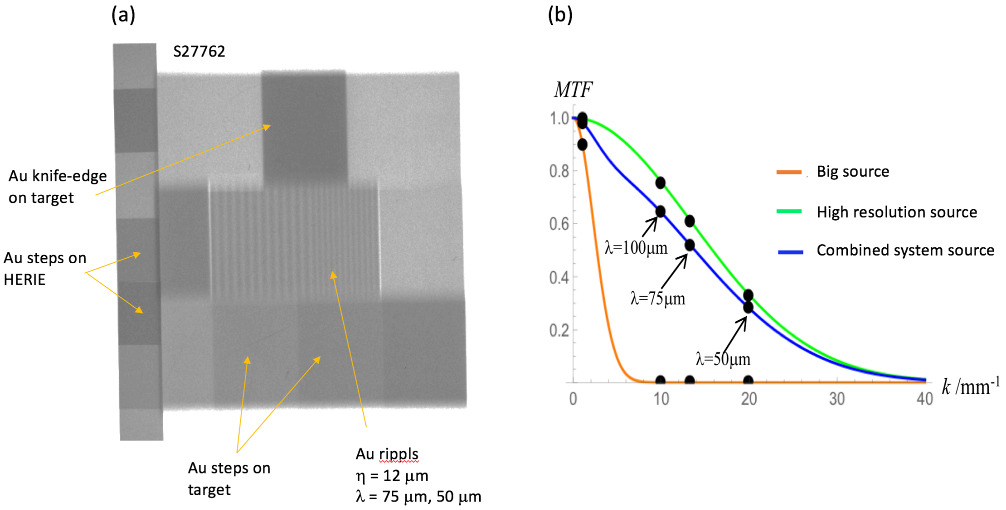

Figure 1. (a) S27762- radiography of known large amplitude ripples and x-ray knife edge. (b) MTF derived from (a) showing inferred contributions from 2 backlighter sources.

[1] E. Gumbrell, J. M. McNaney, C. M. Huntington, A. G. Krygier, H. -S. Park, "Characterizing the modulation transfer function for x-ray radiography in high energy density experiments", *Rev. Sci. Instrum.*, **89**, 10G118 (2018).

D. National Security Applications

1. SolarCellESD: Solar Cell Electrostatic Discharge Experiments (PI: K. Widmann)

with Phil Jenkins (NRL), Steve Seiler and Heather Jiles (DTRA), Patrick Poole and Brent Blue (LLNL)

The SolarCellESD campaign seeks to determine experimentally whether prompt x-rays can induce failure modes in solar arrays that are not accounted for by simply testing the individual solar cells alone, because the voltage difference between neighboring cells can be 100s of volts depending on the overall layout of the array. These experiments at OMEGA have been fielding the smallest possible array, i.e., 2x1 cells with electronic controls that allow the user to dial in a voltage difference (bias voltage) between the two cells and, thus, to study the failure modes as a function of incident x-ray flux, and bias voltage, respectively. The FY18 campaign continued using the partial EMI shield previously tested during the FY17 campaign, and added the option of installing permanent magnets in the front of the enclosure to deflect charged particles, mainly electrons, away from the solar cell samples.

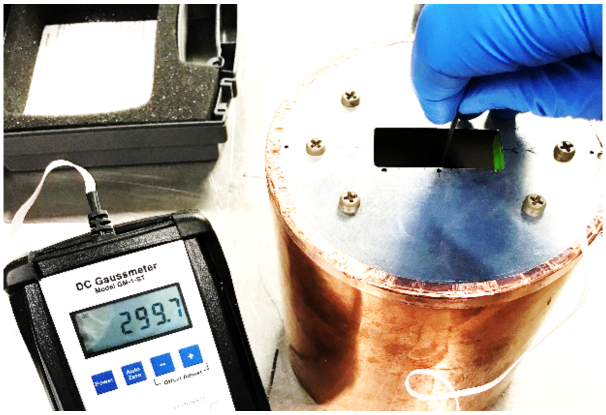

Figure 1: EMI enclosure with permanent magnets installed behind the x-ray aperture. The resulting magnetic field strength is 300 Gauss at the center and over 2000 Gauss near the edge of the aperture.

The laser-driven x-ray source of choice for these solar cell experiments remains the small gold halfraum (600-µm diameter, 600-µm long) but without the pinhole on the closed end. After having demonstrated x-ray induced sustained arcing for the first time during the FY17 campaign, the conditions indicated that it was not necessary to keep the very low-flux option for these x-ray sources. One additional variation in the experimental configuration for the FY18 shots was the view angle between the x-ray source and the solar cell samples. The FY18 shots tested view angles of approximately 35°, 45°, 60°, and 70°, respectively. Post-shot inspections of the solar cell samples indicated a strong dependence of debris on the view angle. Especially at 70°, significant changes are seen in the surface conditions of the area that was exposed to the x rays through the x-ray aperture. Figure 2 shows a before-and-after comparison of one of these solar cell sample coupons, in which one can clearly see the shadow cast onto the surface by the two Langmuir probe tips that are in front of the solar cells. In contrary, shots where the view angle was 35° and 45° didn't have any visible alteration of the surface of the solar cells.

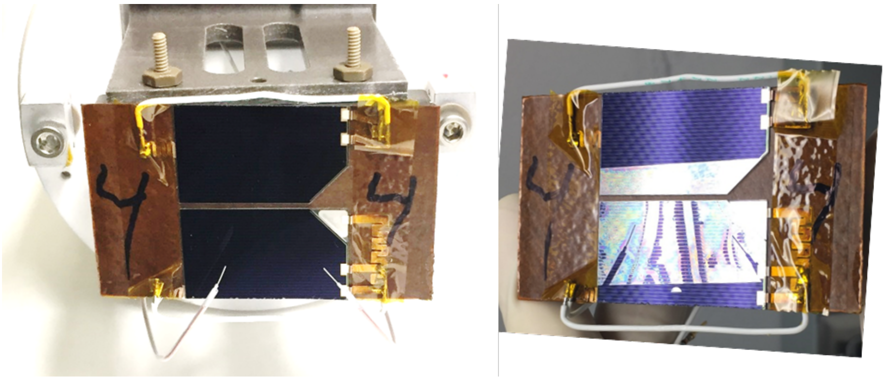

Figure 2: (a) Solar cell array with two Langmuir probes before a shot; (b) The same solar cell coupon after the shot shows significant amount of debris in the area that is exposed to the x rays. The shadow of the Langmuir probe wire tips can be seen in the bottom left and bottom right corners of the "coated" area of the solar cells.

The FY18 campaign was able to further constrain the parameter space with respect to x-ray flux and bias voltage that causes x-ray induced, sustained arcing between the solar cells. By comparing the results obtained with and without the magnetic field at the x-ray aperture, it was also confirmed that the impact of charged particles from the laser-generated plasma is negligible compared to the x-ray induced effects.

2. Plasma Instability Control to Generate High Energy Bremsstrahlung X-ray Source (PI: P. L. Poole)

with R. Kirkwood, S. C. Wilks, M. May, K. Widmann, and B. E. Blue

FY18 continued a campaign to develop a high fluence x-ray source in the 30 – 100 keV range by optimizing plasma instabilities. High fluence sources at lower energies are currently used for materials effects studies in extreme environments, but no good source exists for 30+ keV x-rays. This project aims to enhance laser conversion to plasma instabilities like Stimulated Raman Scattering (SRS) and Two-Plasmon Decay (TPD) which accelerate electrons in plasma waves that will convert to high energy x-rays via bremsstrahlung in the high-Z hohlraum wall.

Two half day campaigns during FY18 explored the effects of different hohlraum fills and the resulting plasma environment on backscattered light and hard x-ray emission. A critical goal was the ability to control which plasma instability was dominant in the plasma between SRS and TPD, and which could be optimized to produce the strongest hot electron spectrum. Figure 1 summarizes this effort, showing the SRS backscatter signal time resolved and compared to the hard x-ray signal: hohlraums with inner CH lining were dominated by the SRS interaction and emitted the hardest x-rays late in the drive pulse. The foam-filled targets instead produced conditions optimum for TPD, generating all energies of x-rays early in time before any SRS backscatter initiated. Additionally, C_5H_{12} gas fills were studied on the same hohlraum designs (demonstrating low hard x-ray yield but providing a critical comparison of the CH-lined and foam-filled results to historical data), as well as a range of foam densities to investigate scaling.

The results from the Omega campaign were used to design a complementary NIF shot day in Q2 FY18, which achieved the same hard x-ray signal as the previous but used only 40% of that laser energy. The campaign is now focused on using subsequent Omega days to optimize plasma conditions for SRS with more unique targets, including foam fills with density gradients, but the initial success has led the next planned NIF shots to include samples to be studied under this unique hard x-ray environment, despite still being in the source development phase. As such these FY18 results have reached the cusp of a new x-ray source which will represent a large capability increase for National Security Applications and related materials under extreme conditions studies, with the additional benefit of broadening the understanding of plasma instability control for fusion and other applications.

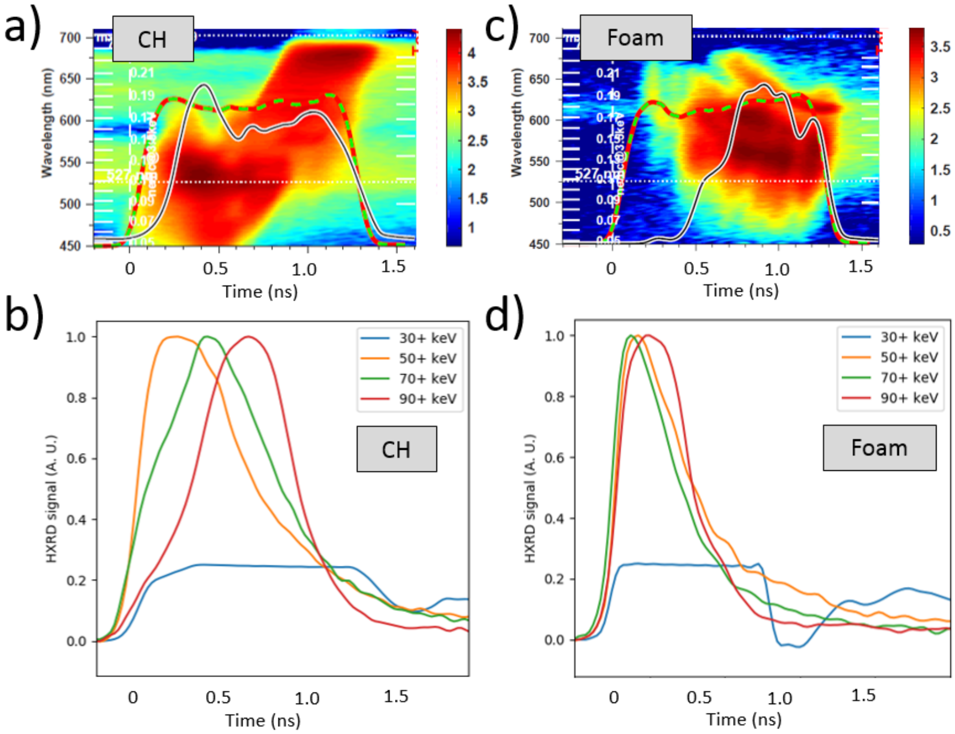

Figure 1: Time-resolved SRS backscatter data (a) and hard x-ray signal (b) for CH-filled hohlraum, increased x-ray emission at later times and higher plasma densities. By contrast, the foam-filled targets show only late-time SRS backscatter (c) and a corresponding drop in x-ray signal (d) at those times.

3. Enhancing Multi-KeV Line Radiation from Laser Driven Non-Equilibrium Plasmas through Application of External Magnetic Fields (PI: G.E. Kemp[1])

with P.L. Poole[1], D.A. Mariscal[1], G.F. Swadling[1], J.D. Colvin[1], K.B. Fournier[1], M.J. May[1], A. Dasgupta[2], A.L. Velikovich[2], J. Giuliani[2], C.K. Li[3], A. Birkel[3], and B.E. Blue[1].
1 Lawrence Livermore National Laboratory, Livermore, CA 94550, USA
2 Plasma Physics Division, Naval Research Laboratory, Washington, DC 20375-5346, USA
3 Plasma Science and Fusion Center, Massachusetts Institute of Technology, Cambridge, MA 02139, USA

A recent LLNL LDRD effort (17-ERD-027) has been studying the influence of externally applied magnetic fields on laser-driven x-ray sources – like those typically used for high fluence radiography or backlighters – with the ultimate goal of improving multi-keV x-ray conversion efficiency through thermal transport inhibition. This series of shots was designed to test and qualify a platform for fielding externally generated magnetic fields on previously fielded x-ray sources on the Omega laser facility. This platform is intended to collect data in the 10+ T magnetic field regime, where currently very little data exists for such high-Z, non-LTE, magnetized plasma conditions. The collected data will be used for constraining thermal transport inhibition and magneto-hydrodynamics models currently used in the multi-physics radiation hydrodynamics code HYDRA.

The experimental configuration is illustrated in Figure 1. Thin walled, cylindrical Kr gas-pipes (1.5 atm), Cu foams (~10 mg/cm^3), and Cu hohlraums were driven by 20 kJ of laser energy in a 1ns pulse (40 beams) as typical sources of K-shell line-radiation. A total of 12 shots were taken, half of which had externally imposed B-fields. The pulsed-power Magneto-Inertial Fusion Energy Discharge System (MIFEDS) was used to provide axial external B-fields strengths of roughly 13 T. Quantifying changes in x-ray emission with increasing external B-field strength was the primary goal of the shots, recorded with Dante (0-20 keV), hard x-ray detectors (20-500 keV), pinhole cameras (>2 keV), and the Dual Channel Spectrometer (11-45 keV). Secondary diagnostics included proton radiography and stimulated Raman/Brillouin laser backscatter. A D^{3}He backlighter capsule (driven by the remaining 20 beams) provided a source of 3 and 15 MeV protons. Analysis is ongoing, but initial results suggest 10-30% enhancements in multi-keV Kr emission when the B-field is present, consistent with the pre-shot modeling [1], with only modest changes in laser backscatter. Neither the Cu foams nor cavities showed significant changes in x-ray emission.

Preliminary results from this campaign were presented at the 2018 HEART Technical Interchange Meeting in Tucson, AZ and are being used to further optimize the platform to make more measurements in Q1 FY19 using a dual-MIFEDS configuration, with expected magnetic fields in excess of 20 T.

[1] G.E. Kemp et al., Physics of Plasmas **23**, 101204 (2016).

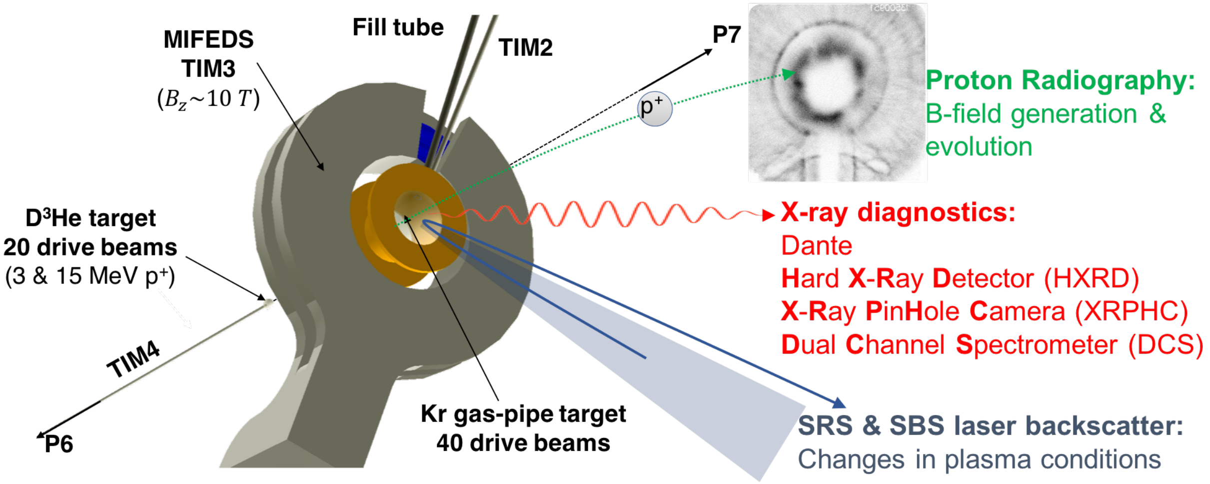

Figure 1. Experimental configuration for MagXRSA-18A. X-ray emission, laser backscatter, and proton radiography data were simultaneously obtained to quantify the evolution and influence of external B-fields in these interactions.

E. *Plasma Properties*

1. Investigation of High Velocity Plasma Flow into a Low-Density Magnetized Background Plasma Region (PI: B.B. Pollock)

with G. Swadling, J.S. Ross, and H.-S. Park

This "Debris Plasma" campaign continued the Magnetized Collisionless Shock – Weapons Effect campaign from previous years. The goal for this series of experiments is to quantify the interaction of high velocity plasma flow into a region containing a low density, weakly magnetized background plasma. This is relevant for understanding the effect of high altitude detonations and the resulting interaction with plasma in the atmosphere. The intent is to compare with both fluid and particle-in-cell (PIC) modeling to determine if a less computationally intensive fluid code can capture enough of the relevant physics to reproduce the data, or if kinetic effects like collisions are required in the simulations (pushing toward a PIC treatment). The field is supplied by the LLE MIFEDS, which delivers 4-8 T at the interaction region of the experiments (depending upon the specific geometry of the MIFEDS coils). The plasma flows originate from two separate foil targets, one of which is mounted to the MIFEDS structure (in either the position occupied by the green foil or the red foil in the figure); the second foil is independently mounted outside the MIFEDS. The foil material compositions, spacing, and plasma arrival time to the interaction region can be varied each shot, as can be the laser drive onto each foil.

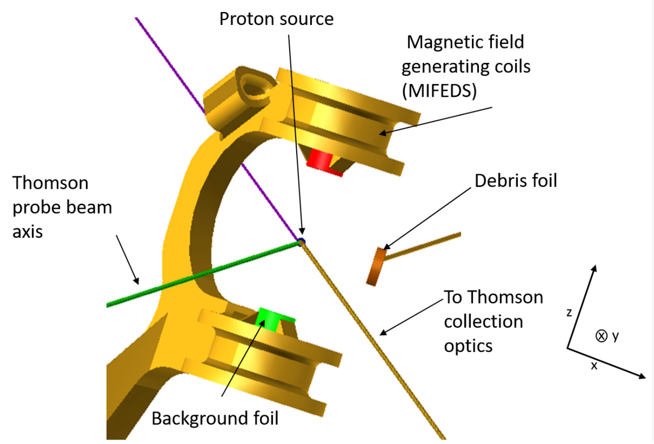

Figure 1. Experimental configuration viewed from the proton detector in TIM1. One or two foils can be mounted to the MIFEDS structure, which is centered at TCC. The TS geometry is k-matched to the z-axis of the experiment. The capsule is 1 cm into the page from TCC, and the debris foil is 2 mm from TCC.

The interaction region of the two flows is simultaneously probed with 2w Thomson scattering and protons from the implosion of a D^3He-filled capsule. Initial measurements of the electron density and temperature from the Thomson scattering do not indicate a strong dependence on the strength or direction of the background magnetic field. The proton deflectometry data do show structural differences in the measured proton distribution with and without the field, but further modeling and simulations are needed in order to quantify these differences. During these experiments the field of view of the proton-probed region has been enlarged significantly by reducing the magnification from ~30 (as in the beginning of the series) to ~10. This was achieved by inserting the CR-39 detector to ~11 cm from the target chamber's center, and allows the entire region between the MIFEDS coils to be visible in the proton data.

2. Measurement of Gold Thermal Transport and M-shell Emission Using a Buried Layer Platform (PI: E.V. Marley)

with L.C. Jarrott, M.B. Schneider, G.E. Kemp, M.E. Foord, R.F. Heeter, D.A. Liedahl, K. Widmann, C.W. Mauche, G.V. Brown, J. Emig

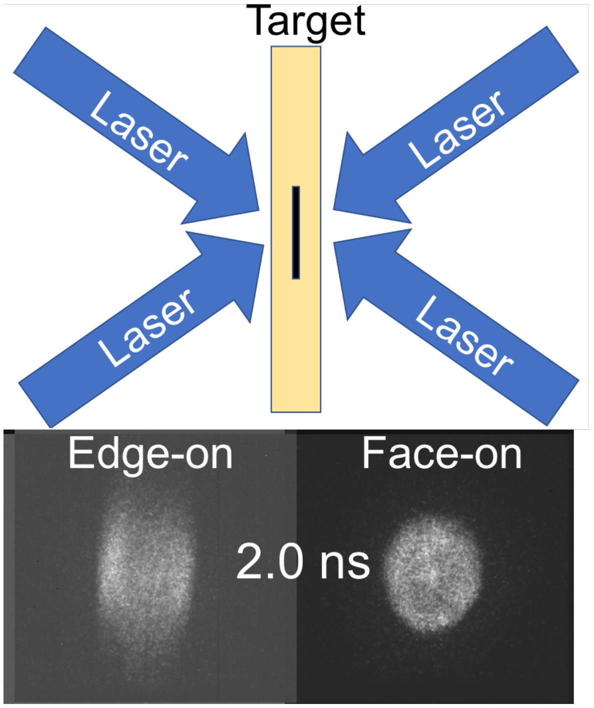

Figure 1. Experimental configuration and pinhole images of the emission area at 2.0 ns of shot 89435.

This campaign was designed to measure the thermal transport through gold layers as well as measure the emitted M-shell gold spectra from a well characterized and uniform plasma for comparison to atomic kinetic models. The buried layer target geometry used for this experiment is capable of generating plasmas with an electron temperature of ~2 keV at electron densities of 10^{21} electrons per cubic centimeter. These are also the conditions found inside gold hohlraums used on experiments at the National Ignition Facility (NIF), providing a stable laboratory setting for radiation transport and atomic kinetic studies.

Planar, buried layer targets were illuminated equally on both sides (Fig. 1) to heat the sample. Two sample types were used during the campaign. The first was a 700 Å thick Au/V mixture designed to burn through completely before the end of the laser pulse, providing uniform plasma conditions to measure the M-shell emission of the gold. The second sample type was composed of 3 layers: the outer two layers were 500 Å thick Au while the final central layer was 600 Å Sc. These targets were designed to measure the thermal transport of Au using the K-shell emission of the Sc. Both sample types were buried between two 5 µm thick layers of Be which acted as an inertial tamp slowing the expansion of the sample.

Time resolved 2-D images of the target's x-ray emission, viewed both face on and side on, were recorded using pinhole cameras coupled to framing cameras (see figure 1 lower). The K-shell spectra from the Sc and V was used to determine the electron temperature of the plasma. The time resolved spectra was recorded using a crystal spectrometer coupled to a framing camera as well as a crystal spectrometer coupled to an x-ray streak camera. Two crystal spectrometers were used to record the full range of the Au M-shell emission, also time resolved. All of the framing cameras used, those for imaging as well as those used for spectroscopy, were co-timed so the plasma conditions could be determined for the measured Au M-shell emission.

There were two different pulse shapes used to determine the most efficient for coupling laser energy into the buried layer target. A 3.0 ns square pulse and a 3.0 ns square pulse with a 100 ps picket arriving 1 ns before the main pulse. A complete (All 6 diagnostics, correctly timed) set of data was recorded for both target types, using both pulse shapes during the campaign at temperatures ~2 keV.

F. Hydrodynamics

1. Experiments of Single-Mode Rayleigh-Taylor Growth in the Late-Nonlinear Stage, and Dependence on Density Contrast. (Shot PI: L. Elgin, U. Michigan*)

with C. Huntington (LLNL), T. Handy, G. Malamud, S. R. Klein, M.R. Trantham, R.P. Drake, A. Shimony and C. C. Kuranz (U Michigan)

* This work funded by Lawrence Livermore National Laboratory under subcontract B614207.

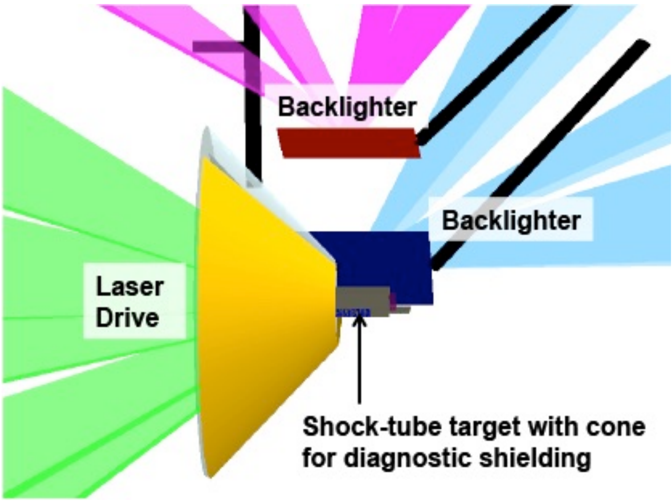

Figure 1. Experimental configuration

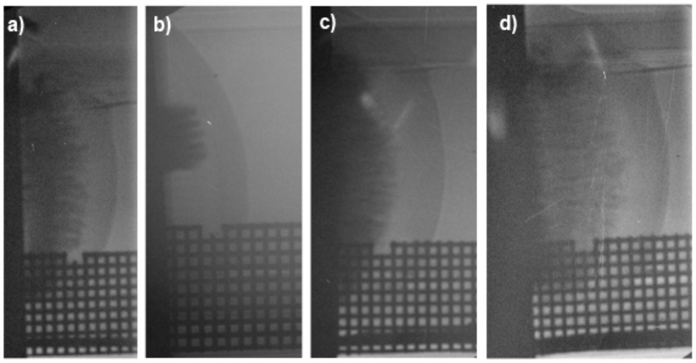

Figure 2. Radiography data of 3D λ = 40 µm low-A targets: a) RID 90385 at 20 ns; b) RID 90387 at 20 ns; c) RID 90381 at 25 ns; d) RID 90382 at 30 ns.

This campaign completed four shot days in FY17-FY18 to observe the evolution of single-mode Rayleigh-Taylor instability (RTI) growth from the early nonlinear stage to the transition to turbulent mixing, in both low- and high-Atwood-number systems. Potential flow models of classical RTI growth predict that spikes and bubbles will reach a terminal velocity. When the density contrast of the two fluids is small, numerical simulations show an unexpected re-acceleration of RTI growth in the late nonlinear stage [1]. Prior experimental studies of single-mode RTI growth have not created the conditions necessary to observe or refute the behavior in question, which requires large aspect ratios of the spike and bubble amplitudes to the perturbation wavelength $(1 \leq h/\lambda \leq 3)$.

In these experiments, a planar blast-wave drives RTI growth at an embedded interface seeded with a single-mode pattern. Target variations include 2D and 3D perturbations and post-shock Atwood numbers of 0.17 and 0.6. A series of X-ray radiographs along dual orthogonal axes captures the evolution of RTI growth. FY17 shots successfully demonstrated dual-axis radiography capabilities with ~10-micron spatial resolution and observed RTI growth in high-Atwood (A=0.6) targets with 3D λ = 40 µm spikes and bubbles. FY18 shots obtained data in low-Atwood (A=0.17) targets with 2D and 3D perturbations and extended the high-Atwood data sets. Results from the FY17 experiments were presented in several venues [2], and FY18 results will be presented at APS DPP 2018 and thereafter.

[1] P. Ramaprabhu *et al.*, Phys. Fluids **24**, 074107 (2012)
[2] L. Elgin *et al.* presentations at APS DPP, Oct. 2017, Milwaukee, WI; NIFUG, Feb. 2018, Livermore, CA; OLUG, April 2018, Rochester, NY; ZFSW July 2018, Albuquerque, NM

2. Development of Novel Diagnostic and Target Fabrication Techniques for X-Ray Imaging of Rayleigh-Taylor Instabilities (PI: C. M. Huntington)

with S. Nagel, K. Raman, J. Bender, S. Prisbrey

“Foam Bubbles” is an ongoing effort to improve target and diagnostic methods for imaging of planar hydrodynamic interfaces. In these experiments a hohlraum is used to drive a plastic ablator package, launching a shock wave into the plastic. The high-density plastic ablator (1.43 g/cc) is paired with a low-density foam (80 mg/cc CRF), creating an interface that is unstable after the passage of the blast wave. The primary diagnostic for this campaign has been point-projection x-ray radiography, and the targets have been optimized for contrast at the 9 keV He-α line from zinc. Previous shot days have used this configuration to develop foams with novel x-ray transmission properties and to maximize shock planarity across the interface.

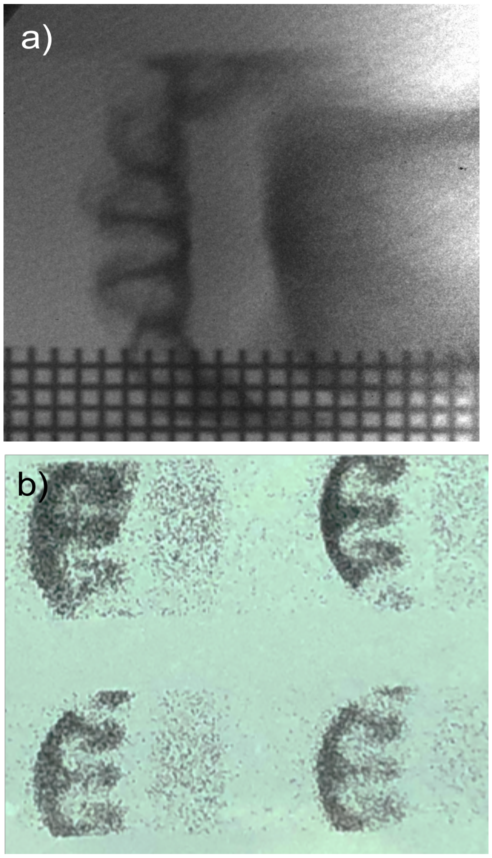

Figure 1. a) Example image from the point-projection x-ray radiography dataset. In this image the unstable interface is being driven from right-to-left, and dark Rayleigh-Taylor spikes can be seen penetrating into lighter, x-ray transmissive foam. b) Example image from the KB, with clear evidence of RT spikes, which are light-colored in this film negative photograph.

There were two principal goals of the September 2018 shot day. A range of targets were prepared with different interface initial conditions, including single-mode (sine wave), multimode (roughened), and flat initial interfaces, to quantify the relative growth of different initial conditions. Additionally, several shots were used to image the system with the Kirkpatrick-Baez (KB) “fixed” diagnostic, which boasts a higher resolution than point projection backlighting, though at a lower energy. Excellent data was collected in the point-projection dataset (Figure 1a), capturing high-resolution data for all target types of interest. The first images of a hydrodynamically unstable planar interface were also recorded with the KB diagnostic (Figure 1b), demonstrating the viability of the technique. With targets optimized for the KB diagnostic (thinner, with higher x-ray transmission at lower energy, to improve data signal-to-noise), it’s anticipated that this instrument will be able to record high-resolution images of hydrodynamic instabilities in future Foam Bubbles campaigns.

3. Mix Width Measurements in Metallic Foams (PI: D. A. Martinez)

with S.F. Khan, M. Rubery, T. Dittrich, S.G. Glendinning, T. Woods, J. Ward, M. Arend, R. Wallace, and T. Baumann

This experiment series was designed to determine which foam manufacturing technique for 0.9g/cc Cu foam produces the smallest mix width for use in hydrodynamics experiments on the NIF. The two Cu foam techniques have a different structure but a primary pore size of ~1μm. In addition, the experiment assessed a Ta_2O_5 foam at 0.9g/cc to determine if a smaller cell size (estimated between 10-100nm) will produce a smaller mix width compared to the Cu foam.

This Joint experiment used a half-hohlraum connected to a shock tube. The shock tube consisted of a polyethylene ablator, a metallic foam sample either Cu or Ta_2O_5 at 0.9 g/cc and followed by a 50mg/cc CRF foam reservoir. The hohlraum was driven using 12 beams with a 1ns square pulse to produce a peak radiation temperature of 200eV. The resulting blast wave causes the metallic foam/reservoir interface to become unstable resulting in RT instability growth. The shock tube was imaged using a point projection backlighter technique with a 10μm diameter Ag wire on a polystyrene substrate and illuminated with the Omega EP short pulse beam. The interface mix was characterized by 90-10% transmission contour between the CRF-sample interface. Figure 1a shows a typical radiograph obtained during the experiment. The interface position was estimated using the Au washer around the shock tube (seen as the dark band on the bottom of figure 1a) and the position of the steepest gradient at the interface. The mix width was measured at 15ns, 19ns and 23.5ns for the Cu foam samples and the Ta_2O_5 was imaged at 23.5ns from the start of the Omega laser drive. Figure 1b shows preliminary measurements of the mix width as a function of interface position. The AWE and GA copper foams produced similar mix widths, suggesting the mix width is insensitive to the micron scale structure of the foam. Although only one data point was obtained for Ta_2O_5, the measured mix width follows along the Cu foam trend, which could also confirm that mix width is insensitive to the internal structure of the foam. Further work is required to confirm these observations.

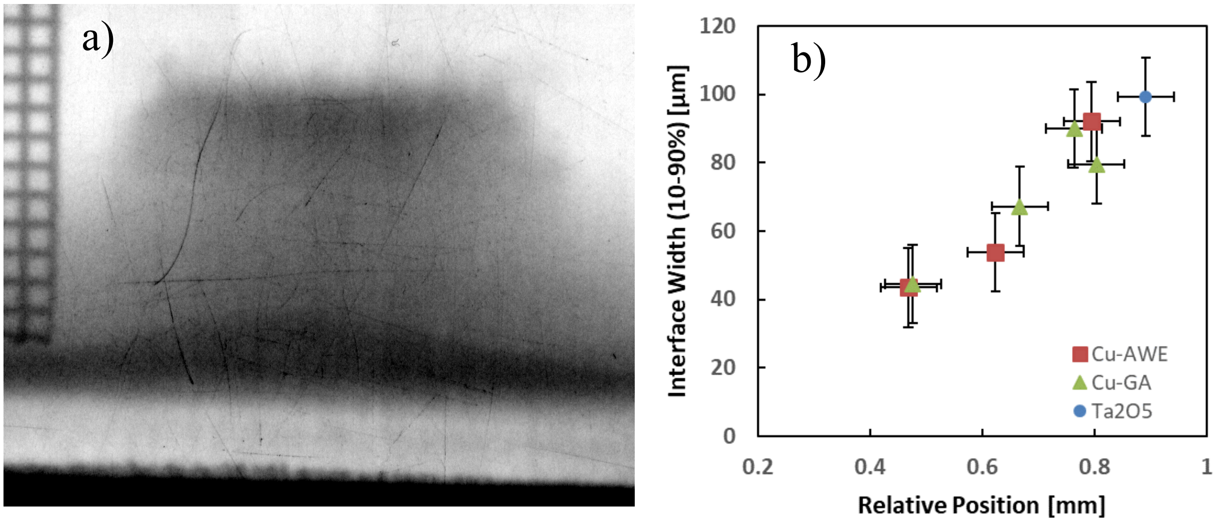

Figure 1: a) background subtracted radiography of AWE Cu foam (shot 90839) at 23.5ns. b) Measured mix width as a function of interface position extracted from the radiographs.

4. Carisbrook Radiography-Velocimetry Campaign (PIs: M. Rubery & D. Martinez)

with S. McAlpin, W. Garbett, G. Glendinning, T. Dittrich & S. Prisbrey

A full shot day on the Omega laser system in September continued the LLNL/AWE Carisbrook campaign. This platform consists of a halfraum with shock tube package, driven using 15 x 500J beams along the Omega H7 axis as shown in Figure 1. The objective was to diagnose the evolution of a hohlraum-driven interface using simultaneous point-projection x-ray radiography and VISAR. The FY18 shots extended data from FY16 and FY17.

To generate the 7.8 keV (4.95 keV) He-alpha point projection x-ray source, a 600 micron square nickel (titanium) microdot was driven to ~2x10^{15} W/cm^2 using 4 x 400J 1ns backlighter beams. The x-ray emission is projected through a 20 um Ta pinhole plate aligned along the shock tube and towards the TIM 6 cranked snout axis of $\theta = 123.1$ and $\phi = 172.76$. Images are recorded on film using a gated x-ray camera (XRFC). Titanium was used instead of nickel on two shots to produce higher contrast in one region of the shock tube package.

A quartz window, aluminum flash coating and light shield cone on the rear of the target enable simultaneous VISAR measurements along the TIM-5 H14 axis. Figures 2 (left) and (right) show good quality VISAR streak camera images from shots 91078 and 91085, with similar targets.

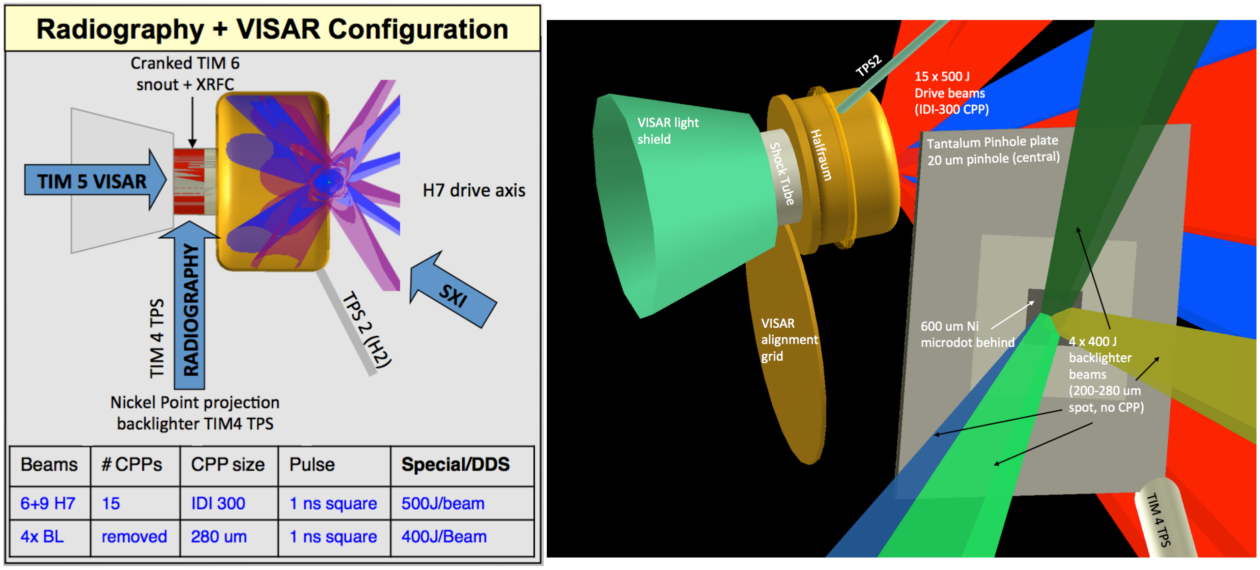

Beams	# CPPs	CPP size	Pulse	**Special/DDS**
6+9 H7	15	IDI 300	1 ns square	500J/beam
4x BL	removed	280 um	1 ns square	400J/Beam

Figure 1. (a) Radiography + VISAR configuration overview. (b) VISRAD isometric view of the experiment.

The shot day returned excellent data on both primary diagnostics. The reproducibility is sufficient for the physics goals of the campaign. Initial analysis of suggests the results are sufficient to close out the Carisbrook Omega effort and begin scaling up the platform to NIF.

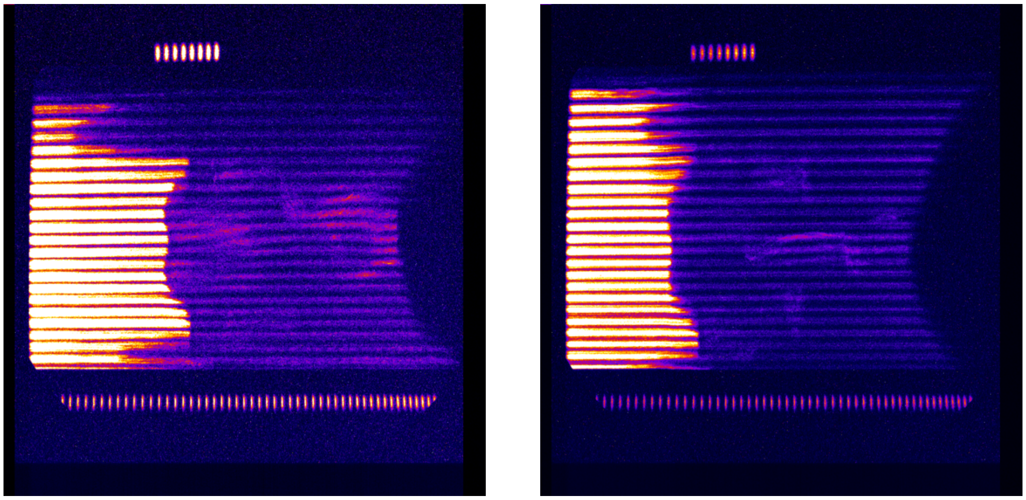

Figure 2 – VISAR streaked images from Omega shot 91078 (left) and 91085 (right).

5. Interaction of Dual High-Energy Backlighters (PI: S.F. Khan)

with D.A. Martinez, S.C. Wilks, S. Prisbrey, S.G. Glendinning, D.T. Woods, and T. Dittrich

The objective of these Omega EP experiments is to study the interaction between dual wire backlighters, a configuration required for campaigns at the National Ignition Facility (NIF). At NIF, the wires will be used for point projection radiography of an indirectly driven spherical implosion of a large target. With the large field of view (>3mm), and the long time interval required between the two sources (>3ns), some degradation of the second wire is expected due to the energy from the first wire. These Omega EP experiments used two 12.5µm diameter Ag wires with a separation of 4mm. Each wire was illuminated by infrared 50ps, 1kJ short pulses. The time interval and order of wire illumination were varied from 0-7.5ns.

It was found that the resolution obtained from the second hit wire was degraded from 19µm to 28µm with a time interval of 5ns (Figure 1). Fourth-harmonic shadowgraphs of the second wire before it was illuminated (Figure 2) show an expanded material diameter of ~37µm at 5ns, larger than the resulting resolution from the wire. This could indicate that the emission distribution from the wire is non-uniform. Further analysis as well as simulations are ongoing. The results from this experiment will be used to design shielding for additional backlighter development experiments at NIF.

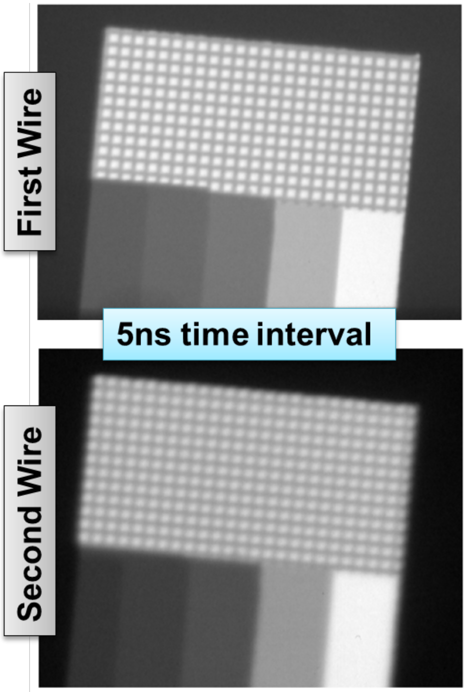

Figure 1. Resolution grid X-ray radiographs from two sequential backlighters.

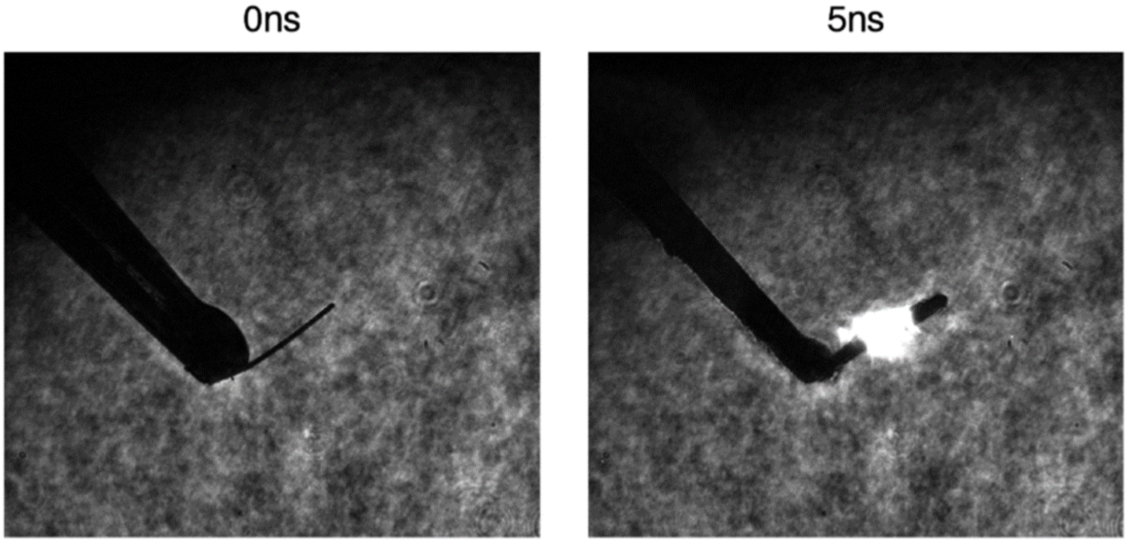

Figure 2: Shadowgraphs of the second wire using the fourth harmonic probe beam.

6. Measurements of Preheat and Instability Reduction with Tamping Layer Relevant to NIF DoubleShell Designs (PI: Y. Ping)

With V. Smalyuk, P. Amendt, R. Tipton, S. Prisbrey, O. Landen, F. Graziani

The goal of this campaign is to identify sources of preheat and reduction of instability growth using tamping layers under conditions relevant to the double shell design on NIF. The target consists of an ablator, CRF foam and a Cu shell attached to a halfraum. Two half-days were fielded, with a total of 11 shots. For the preheat study, time-resolved side-on X-ray radiography was employed with the TCS hard X-ray spectrometer. A clear correlation was observed between the preheat and gas fill as shown in Fig. 1, indicating that hard x-rays generated by laser-plasma interaction in the halfraum contributed to the preheat. For instability growth measurements, ripples with 30um and 60um periods and 1.5um were imprinted on the Cu inner surface and face-on x-ray radiography with framing camera was employed to measure the ripple growth over time. Data analysis (Figure 2) shows less growth with an Al tamping layer than without one.

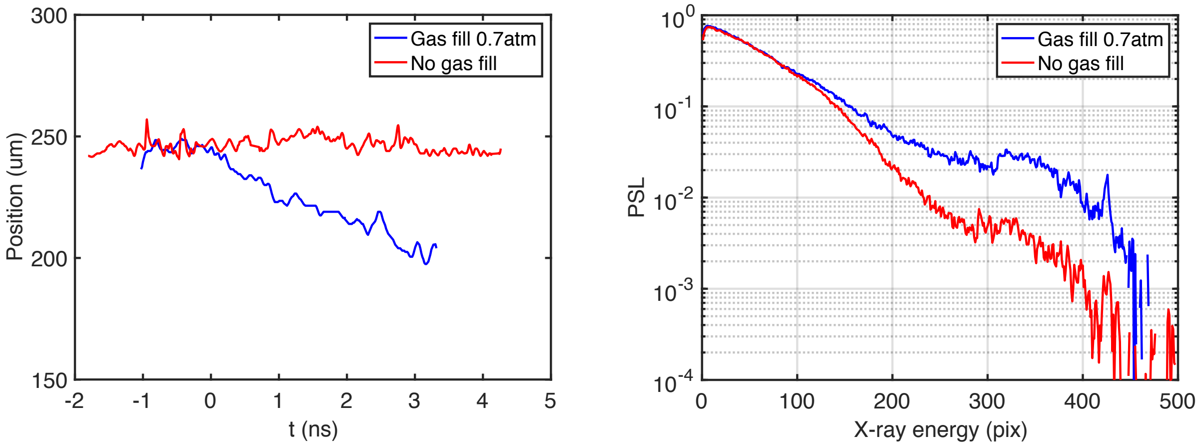

Figure 1. (Left) Position of Cu shell vs time before shock arrival. (Right) Hard x-ray spectra with and without gas fill in halfraum.

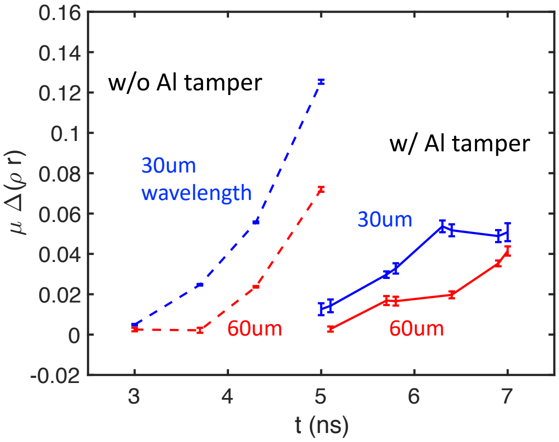

Figure 2. Amplitude of ripples vs time with and without Al tamping layer.

Laboratory Basic Science Experiments

1. Measurement of the High-Pressure Thermal Conductivity of Iron and Titanium (PI: R.F. Smith) with J. Wicks and C. Krill (Johns Hopkins Univ.)

High-pressure thermal conductivity is one of the most important and yet most difficult to measure physical properties of materials. Within the Earth's interior the thermal conductivity, k, of Fe and Fe-rich alloys at core pressure-temperature conditions (135-360 GPa, 2500-5000 K) is a key parameter for heat transport models and plays an important role in determining the temperature profile and energy balance of our planet. The thermal conductivity of the Earth's core remains poorly constrained because of the extreme difficulty in making thermal transport measurements under the relevant pressure and temperature conditions. Two experimental studies published in Nature in 2016 report values of k for Fe which vary by a factor of seven at ~130 GPa (34 → 225 W m^{-1} K^{-1}) [1][2]. The goal of these experiments is to constrain the thermal conductivity at high pressures, using a ramp compression platform previously developed on Omega [3] (Fig. 1,top). Here, fifteen beams deliver 200-300 J over 2-ns into a hohlraum. This results in a shock wave which propagates through the Be/12% Br-CH layer. After shock breakout, the ionized CH unloads across a vacuum gap as piles up against the stepped Fe layer. This results in a mechanical pressure wave and a thermal wave running longitudinally through the sample. The ASBO/SOP diagnostic provides velocity and thermal transport information through the stepped-samples (Fig. 1, middle/bottom). Analysis is underway to translate this data into a measurement of thermal conductivity.

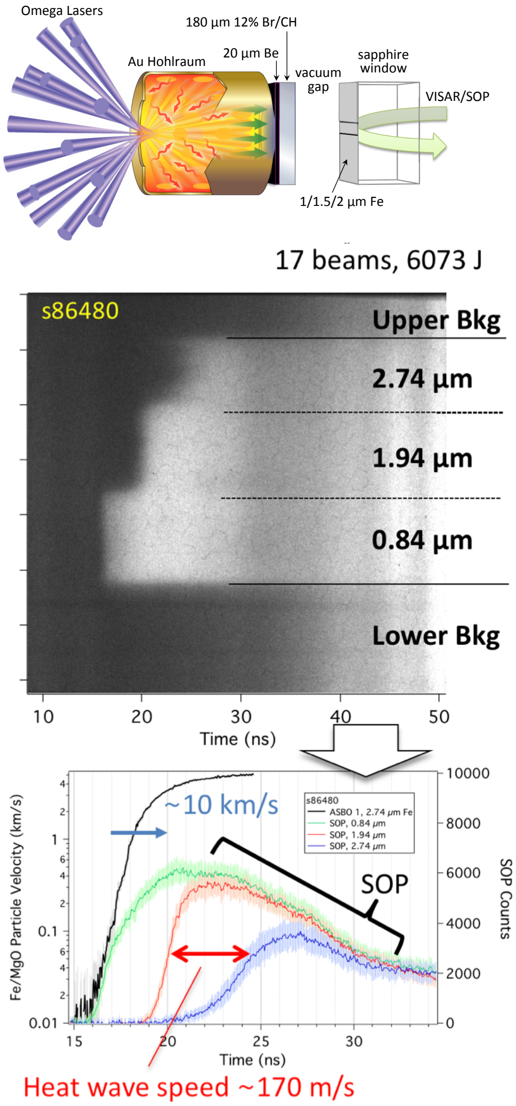

Figure 1. (Top) Target design to measure heat flow in a ramp compressed stepped-Fe sample. (Middle) Raw SOP data shows the heat flow through multiple Fe thicknesses. (Top) Extracted velocity and temperature (SOP counts), both versus time, for different step thicknesses.

[1] Z. Konôpková, R.S. McWilliams, N. Gómez-Pérez and A.F. Goncharov, Direct measurement of thermal conductivity in solid iron at planetary core conditions, Nature **534**, 99 (2016).
[2] K. Ohta, Y. Kuwayama, K. Hirose, K. Shimizu, Yasuo Ohishi, Experimental determination of the electrical resistivity of iron at Earth's core conditions, Nature **534**, 95 (2016).
[3] R.F. Smith et al., "High planarity x-ray drive for ultrafast shockless-compression experiments" Phys. Plas. **14**, 057105 (2007).

2. Probing Heterogeneous Dynamic Fracture and Failure using 2D Velocimetry (PI: S. J. Ali)

with P. M. Celliers, R. F. Smith, J. H. Eggert, D. Erskine

Studies on the timescale and morphology of fracture dynamics, which can occur over μm length scales and timescales of a nanosecond or less, have generated a lot of interest in recent years, but experimental limitations have not permitted simultaneous measurements on these time and length scales [1-5]. This series of shots combines the 1-D (Omega ASBO) and 2-D (OHRV) velocimetry diagnostics to study heterogeneous flow and the formation of fracture networks in diamond. The 1-D VISAR records the compression history of the sample, providing absolute velocity and pressure, while the 2-D OHRV captures picosecond snapshots of the spatially resolved velocity and reflectivity maps.

All four campaign half-days used a half-hohlraum indirect drive to launch a spatially smooth shock wave into either single crystal aluminum, single crystal diamond, or polycrystalline diamond. Over the course of the first campaign, DiamondFailure-18A, it became apparent that the dichroic mirror used to reflect the 532 nm ASBO probe and transmit the 400 nm OHRV probe was being damaged, most likely by unconverted light. This was resulting in distorted images and velocity maps in the OHRV and a loss of reflected light into the ASBO. A redesign of the mirror holding with additional shielding was completed for 18B and refined slightly for 18C and 18D, resulting in a robust platform for making simultaneous OHRV and ASBO measurements with no unusable shots for 18C and 18D.

Overall, the campaign yielded excellent data showing orientation-dependent fracture in the single crystal Al and diamond, and potential intergranular fracture in the polycrystalline diamond. This suggests that over the pressure and strain rate regime observed, the fracture is primarily driven by slip planes in the single crystal samples.

Some initial results, primarily from DiamondFailure-18C are highlighted in Figure 1. In both Fig. 1B and 1D, the single crystal samples, linear features were seen in both the image and velocity map coinciding with the predicted slip plane motion for 100-oriented aluminum and diamond. In the Fig. 1D aluminum data it is also apparent that there is an evolution in the deformation pattern with the most linear features toward the lower left corner, closer to the center of the drive spot and higher in pressure by ~2 GPa relative to the upper right corner. Further analysis is required to determine whether this evolution is a result of time or pressure. In the polycrystalline sample, Fig. 1C, a distribution of features of ~20 microns average size was observed, with lower velocity regions between on the velocity map and discontinuity-like features in the image. As the grain size for these samples is ~10-20 microns, this is commensurate with fracture occurring at the grain boundaries, where the velocity is measurably lower. Results of these campaigns are still being analyzed, with a publication planned for mid FY19.

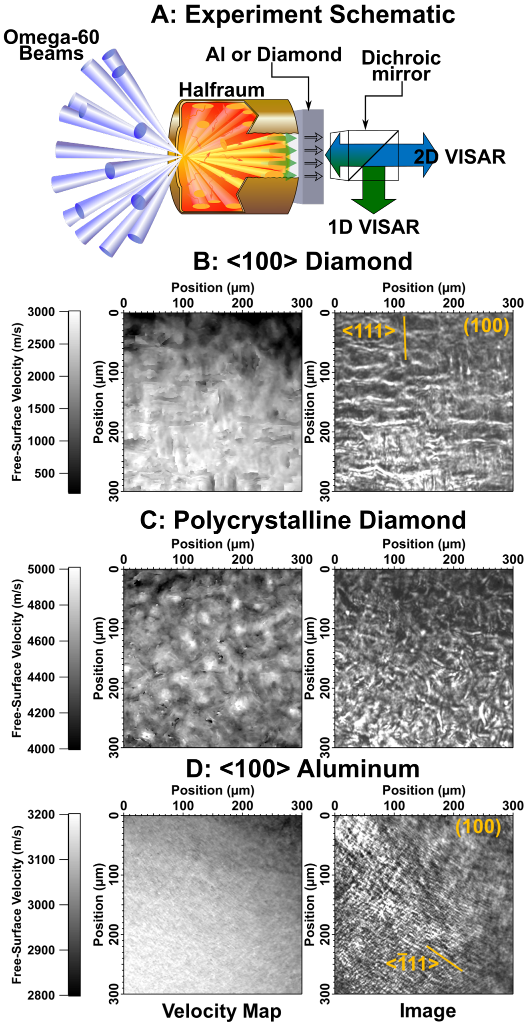

Figure 1. Experimental configuration (A) and OHRV velocity maps and images for 120 GPa single crystal diamond (B), 160 GPa polycrystalline diamond (C), and 30 GPa single crystal aluminum (D).

3. Development of Platform to Benchmark Atomic Models for X-Ray Spectroscopy of Shock-Heated Materials (PI: M. J. MacDonald)

with A.M. Saunders, T. Döppner, C. M. Huntington, H. A. Scott, S. R. Klein, K. Ma, P. X. Belancourt, H. J. Lefevre, K. B. Fournier, W. Theobald, C. C. Kuranz, E. Johnsen, D. S. Montgomery, O. L. Landen, and R. W. Falcone
(Collaboration between LLNL, LANL, LBNL, UC Berkeley, U Michigan and LLE)

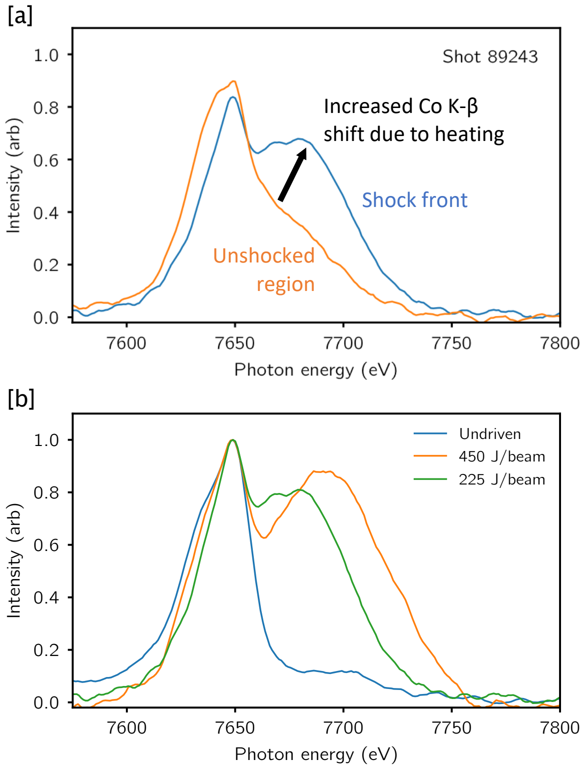

Figure 1: [a] Spatially-resolved Co K-β spectra taken ahead of the shock front (unheated) and at the shock front (heated). [b] Co K-β from unshocked foam (blue) and at the shock front for the full drive showing the largest shift (orange) and half drive with a smaller shift (green).

The FoamXRFTS-18A campaign was the first shot day in a collaboration to develop a platform using simultaneous x-ray fluorescence (XRF) spectroscopy and x-ray Thomson scattering (XRTS) to measure the equation of state of shocked foams. The goal of this platform is to provide XRF spectroscopy data from shock-heated materials at known temperatures, measured independently using XRTS, to benchmark atomic models for future XRF diagnostics.

This platform uses a planar shockwave to heat a cylinder of foam doped with a mid-Z element, similar to previous results published from the Trident laser facility at Los Alamos National Laboratory [1], with the addition of an XRTS diagnostic. A laser-driven Zn He-α backlighter both induced K-shell fluorescence from the Co-doped foam and served as the x-ray source for XRTS. The IXTS spectrometer recorded spatially-resolved Co K-β XRF, measuring the density profile of the shock wave in the foam in addition to resolving XRF spectra from the shocked and unshocked regions of the foam. The Co K-β spectra from the shock-heated layer can be modeled using atomic kinetic and radiation codes to infer temperatures, electron densities, and ionization state distributions. These results will be compared to temperatures measured using the XRTS on the ZSPEC spectrometer to improve atomic models used in XRF modeling at similar conditions. This first campaign demonstrated the ability to spatially resolve XRF spectra in a single shot (Fig 1a) and measure changes in the Co K-β shift by varying the drive intensity (Fig 1b). Shielding issues with the XRTS measurement were resolved by the end of the shot day and a follow-up experiment is planned for December 2018 (FoamXRFTS-19A).

[1] M. J. MacDonald *et al.,* J. Appl. Phys. **120**, 125901 (2016).

4. Laue Diffraction and Recovery of Shocked Single Crystal Quartz (PI: A. Krygier)

with C Wehrenberg, A Gleason, H-S Park, B Remington

As the second most abundant mineral in the continental crust, SiO_2 (quartz) plays a large role in the dynamics of meteor impacts on Earth. Quartz has become the most important material for identifying meteor sites, due to the wide range of permanent shock effects including the formation of polymorphs like Stishovite and Coesite. This campaign performed *in situ* Laue diffraction of shocked high purity single crystal samples, combined with *ex situ* recovery analysis of a range of shocked natural samples, as illustrated in Figure 1. Laue diffraction is a powerful tool for characterizing crystalline lattice dynamics in compressed samples, and recovery analysis enables a wide range of sophisticated materials science techniques.

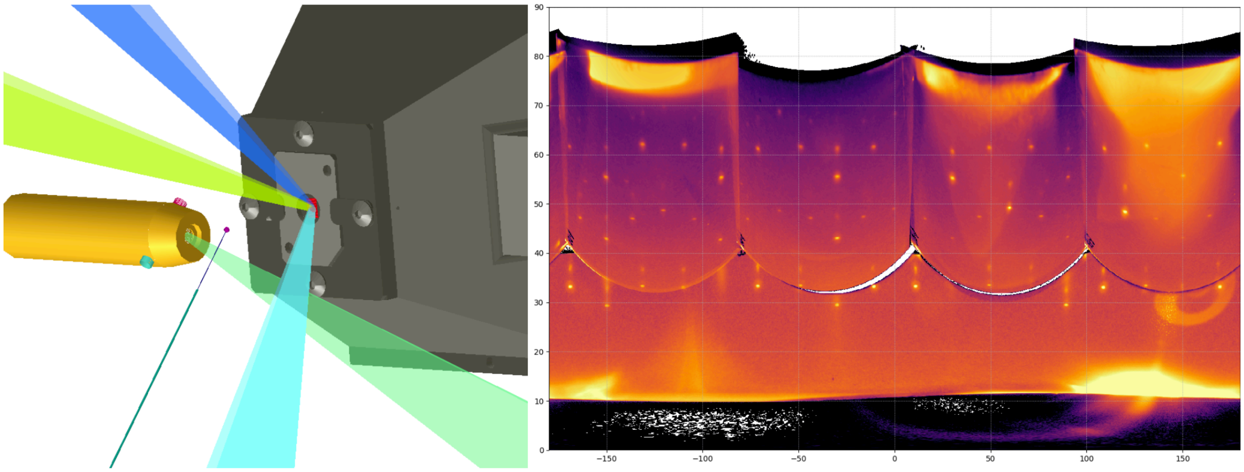

Figure 1. (Left) Experimental setup, with BBXRD Laue diffraction diagnostic (grey) and shock recovery tube (yellow) to recover intact shock-compressed samples for *ex situ* analysis. (Right) Laue diffraction data.

These shots produced Laue diffraction of Z, X, and Y-cut quartz samples shocked to ~10-50 GPa, and recovered natural samples shocked to over 100 GPa. Laue diffraction is a direct measure of the orientation of crystal lattice planes, and the configuration allowed direct measurement of the strain anisotropy during the shock. The X-rays are produced by an imploded CH capsule that generates a smooth, broadband, 100s ps X-ray flash at stagnation. The sample conditions are determined by the Active Shock BreakOut diagnostic, with sample data shown in Figure .

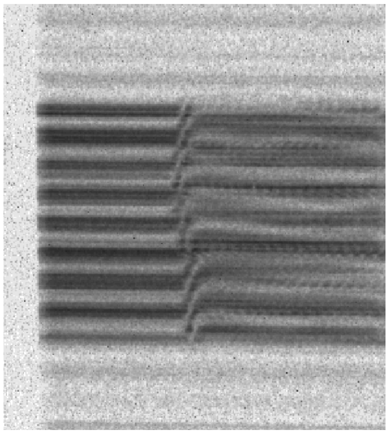

Figure 2. Raw Active Shock BreakOut data.

This experiment yielded 12 shots of extremely high-quality Laue diffraction and successfully recovered samples. Analysis is underway with publications to follow.

5. Time Resolved Measurement of the Radiative Properties of Open L-Shell Germanium (PI: E.V. Marley)

with L.C. Jarrott, M.B. Schneider, G.E. Kemp, M.E. Foord, R.F. Heeter, D.A. Liedahl, K. Widmann, C.W. Mauche, G.V. Brown, J. Emig

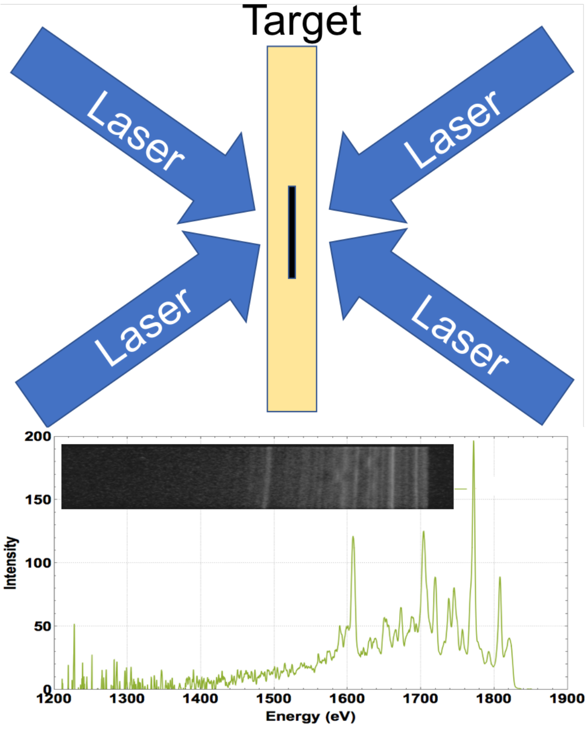

Figure 1. (Top) Experimental configuration. (Bottom) Time Resolved Ge L-shell spectra with data inset at 2.6 ns of shot 90543.

This campaign was designed to measure the emitted L-shell germanium spectra from a well characterized and uniform plasma for comparison to atomic kinetic models. Recent studies have shown a discrepancy between atomic kinetic models and high Z M-shell spectral data. This study was done to test the accuracy of models for L-shell emission.

In two Omega shot days, planar buried layer targets were illuminated evenly on both sides (Fig. 1) to heat the sample, composed of Sc and Ge layers. The first shot day used samples with Ge layers surrounding a single Sc layer in the center. The second shot day placed Sc layers surrounding a single Ge layer. This verified that the target was heating through, and the same conditions could be reached on both shot days. These layers were embedded between two 5 μm thick layers of Be tamper which slows the sample expansion. Time resolved 2-D images of the target's x-ray emission, viewed both face on and side on, were recorded using time-gated pinhole cameras. Gated Sc K-shell spectra from a crystal spectrometer were obtained to determine the electron temperature of the plasma. A second gated crystal spectrometer recorded the Ge L-shell emission at 4 times. During the second shot day, streaked Ge L-shell spectra also provided a continuous record of the ion population shift in time. A third gated spectrometer, which utilized a variably spaced grating and a slit, provided time- and space-resolved Ge L-shell spectra as well, to verify the uniformity of the plasma at different times during the experiment. All of the framing cameras used, for imaging and spectroscopy, were co-timed so the plasma conditions could be determined for the measured germanium L-shell spectra.

The first shot day tested two different pulse shapes: a 3.0 ns square pulse and an identical pulse preceded by a 100 ps picket. The latter was used to generate a pre-plasma before the arrival of the main pulse, creating a smoother interface for the laser-plasma interaction and more efficient coupling of energy into the target. The second shot day used a 3.5 ns square pulse with a picket to deposit the same energy into the target over a longer time. Complete data from all 6 co-timed diagnostics were recorded on both days at temperatures ~1.5 keV. Detailed analysis is in progress and expected to result in future publications.

6. Characterizing Pressure Ionization in Ramp Compressed Materials with Electron Induced Fluorescence (PI: S. Jiang)

with Y. Ping, R. Smith, A. Jenei and J. Eggert

This pressure ionization campaign comprised 1 day on OMEGA EP during FY18. This campaign was designed to measure ionization in compressed Co as a function of density, using the K shell fluorescence spectroscopy. A schematic of the experimental setup is displayed in Figure 1(a). The K shell line emissions were induced by hot electrons generated through short-pulse laser-solid interactions. A large, thick Al target was used to avoid heating from the short pulse. The high pressure was achieved by ramp compression using the long pulse drivers, so that the temperature was kept low during the compression process. During the experiment, the pressure history was characterized with VISAR measurements. The target structure is also shown in Figure 1(a). Despite the Co layer under study, the targets also included a thin Cu layer as energy reference. The shots varied the driver intensities to reach different densities without raising the thermal ionization effect and reached up to 2.0-2.2x compression with maximum long pulse energy. There is still little consensus on pressure ionization under these conditions despite extensive theoretical and experimental efforts.

The main diagnostic used in this campaign was a high-resolution X ray spectrometer IXTS. It successfully measured the Cu K_{α} and Co K_{β} fluorescence lines with high signal to noise ratio as can be seen in Figure 1(b). Under the designed experimental conditions, pressure ionization has a much more prominent effect on the outer M shell compared to inner shells (K, L shells). Therefore, the Cu K_{α} line is predicted to have negligible energy shift, while the Co K_{β} line is more prone to a shift. Figure 1(b) shows the measure Co K_{β} peaks under different compressions. A small red shift was observed under 2.0-2.2x compression, which is contrary to the prediction of the Ecker Kroll ionization model. This campaign provided a direct and unambiguous measurement of the pressure ionization effect for benchmarking various ionization models.

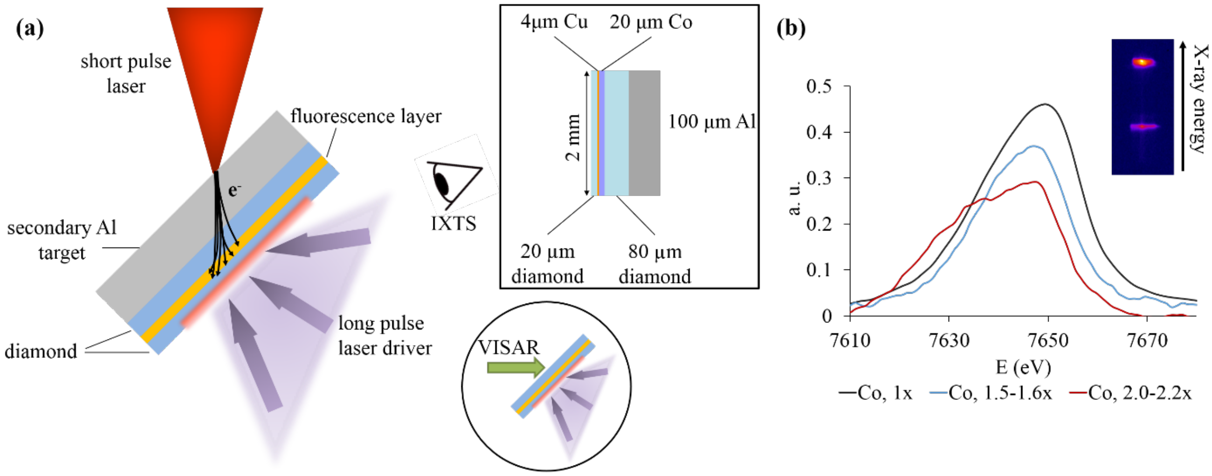

Figure 1: (a) A schematic of the experimental configuration. The inset on top right shows the target geometry. The inset on bottom right shows a schematic of the VISAR configuration. (b) Measured IXTS spectra of Co K_{β}. The lineouts are from different driver conditions. An example of the raw image is shown in the inset.

7. Exploring Pair Plasmas and Their Applications (PI: H. Chen)

In FY18, an LLNL / General Atomics / University of Michigan team carried out the project "Exploring pair plasmas and their applications" with 2 LBS shot days on OMEGA EP. The campaign used an EP short pulse beam to produce jets of electron-positron antimatter pairs while the 2nd short pulse beam was used to producing protons to diagnose the laser-target interactions. The experiments focused on 1) enhancing the pair yield using nano-structured targets and 2) collimating and/or focusing positron jets through curved sheath potentials from shaped target surfaces. The experiments successfully demonstrated both the yield enhancement and the positron focusing. The data provided basis future experiments on laboratory astrophysics using the pair jet – plasma interaction to drive beam instabilities. A total of 14 shots were performed in the fiscal year.

The EP short pulse beams (~1 kJ in 10 ps) irradiated targets of 1 mm thick Au targets, with and without the nano-structure on the laser interaction surface. It was found that for the same laser energy, positron yields and acceleration both were increased dramatically by using nano-structure [1]. This finding is important to the future experiments and applications using laser pair jets. Previous experiments used gold targets almost exclusively. It was also found that a hemispherical shaped back surface can focus the positron jets through the sheath field – similar to that observed in proton focusing. This observation is important as it demonstrated that higher pair density can be achieved by reducing their volume, which may enable the development of instabilities predicted by theory.

The prior experiments showed that quasi-monoenergetic relativistic positron jets are formed during high-intensity irradiation of thick gold targets [2, 3], and that these jets can be strongly collimated [4] using the magnetized-inertial fusion electrical delivery system (MIFEDS) [5]. The external field produces a 40-fold increase in the peak positron and electron signal [4]. The positron yield was found to scale as the square of the laser energy [6, 7]. The FY15 results revealed another dimension of scaling on the target materials. The favorable scaling would enable the laboratory study of relativistic pair plasmas that are important to understanding some of the most exotic and energetic systems in the universe [7, 8].

[1] J. Sheng, et al., to be submitted.
[2] H. Chen et al., Phys. Rev. Lett. **102**, 105001 (2009).
[3] H. Chen et al., Phy. Rev. Lett. **105**, 015003 (2010).
[4] H. Chen et al., Phys. Plasmas **21**, 040703 (2014).
[5] O. Gotchev et al., Rev. Sci. Instrum. **80**, 043504 (2009).
[6] H. Chen et al., Phys. Rev. Lett. **114**, 215001 (2015).
[7] H. Chen et al., Phys. Plasmas **22,** 056705 (2015).
[8] H. Chen et al., High Energy Density Physics, **7**, 225 (2011).

8. Astrophysical Collisionless Shock Experiments with Lasers (ACSEL) (LBS PI: H.-S. Park; Shot PI: B.B. Pollock)

with G. Swadling, J.S. Ross, and H.-S. Park

The goal for ACSEL-O18A is to quantify the interaction of orthogonal plasma flows with and without a background magnetic field. The field is supplied by the LLE MIFEDS, which delivers 4-8 T at the interaction region of the experiments (depending upon the specific geometry of the MIFEDS coils). The orthogonal plasma flows originate from two separate foil targets, one of which is mounted to the MIFEDS structure at one of the positions indicated by the red and green foils in the figure; the second foil is independently mounted outside the MIFEDS structure. The foil material compositions, spacing, and plasma arrival time to the interaction region can be varied each shot, as can be the laser drive onto each foil.

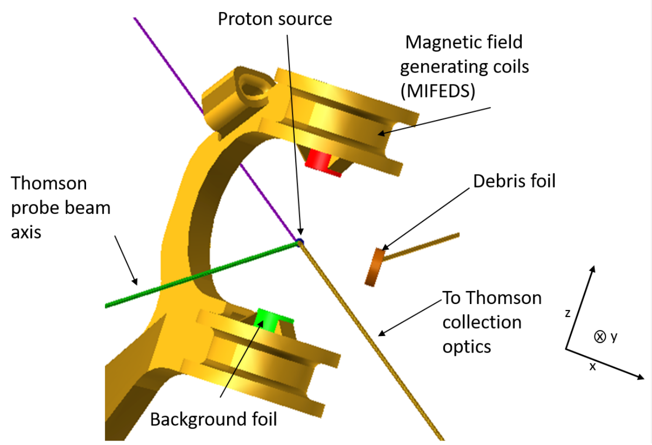

Figure 1. Experimental configuration viewed from the proton detector in TIM1. 1 or 2 foils can be mounted to the MIFEDS structure, which is centered at TCC. The TS geometry is k-matched to the z-axis of the experiment. The capsule is 1 cm into the page from TCC, and the debris foil is 2 mm from TCC.

The interaction region of the two flows is simultaneously probed with 2w Thomson scattering and protons from the implosion of a D^3He-filled capsule. To study the dynamics of these flows, the foil inside the MIFEDS is generally driven with ~500 J of laser light, while the separate foil is driven up to 8 ns later by ~2 kJ. Two types of scan attempted on these shots include varying the arrival time of the protons for given foil drive conditions to map out the temporal evolution of the interaction, and holding the proton probing time fixed relative to the initial foil drive and varying the arrival time of the second plasma. Initial measurements of the electron density and temperature from the Thomson scattering do not indicate a strong dependence on the strength or direction of the background magnetic field. The proton deflectometry data do show structural differences in the measured proton distribution with and without the field, but further modeling and simulations are needed in order to quantify these differences. During these experiments the field of view of the proton-probed region is sufficiently large to allow the entire region between the MIFEDS coils to be visible in the proton data.

9. Proton Isochoric Heating for Warm Dense Matter Studies (PI: D. Mariscal)

with T. Ma, G. J. Williams, H. Chen, S. Wilks (LLNL) C. McGuffey, J. Kim (UCSD)

High intensity proton beams driven by multi-picosecond kJ-scale lasers are an effective means to rapidly heat solid targets into the Warm Dense Matter (WDM) state [1]. Omega EP short-pulse-driven proton beams containing 20-50 J at proton energies >3 MeV can be rapidly (<50 ps) deposited into solid density samples, heating them to >100 eV temperatures before significant hydrodynamic expansion can occur (i.e. solid density).

CH hemispherical targets (15 μm thick x 375 μm radius of curvature) were driven by EP short pulse beams defocused to R_{80}~45 μm at 3, 6, and 10 ps pulse lengths at 800-1000 J in order to focus proton beams to Cu samples (15 or 50 μm thick x 200 μm diameter). A radiochromic film stack and a Thomson parabola instrument were used to monitor the transmitted ion sources for each shot. Both low resolution (Zinc Von Hamos) and high resolution (HiResSpec) x-ray spectrometers measured Cu k-alpha and k-beta emission in order to infer the temperature of the heated samples. At 50+ eV temperatures significant shifts in Cu k-α are expected, and at ~200 eV temperatures Cu k-β shifts and depletion are also expected. The laser pulse length was varied in order to find an optimum between laser-to-proton conversion efficiency and the optimum proton beam spectral characteristics for heating. Additionally, the Cu sample position was moved closer and further from the proton source in order to look for an optimal proton beam focus for heating.

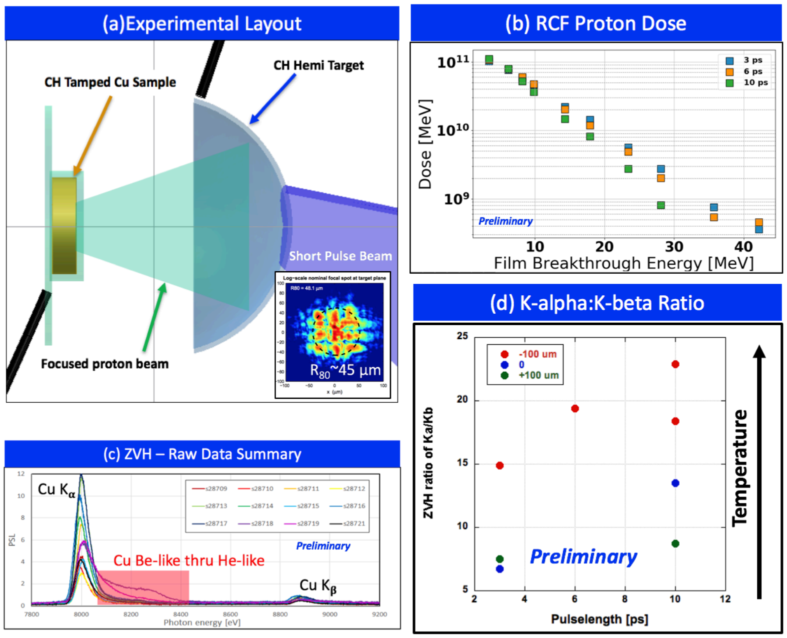

Figure 1. (a) Experimental configuration & defocused laser spot (inset). (b) Transmitted proton dose in RCF stacks showing differences in proton beam spectra vs. pulse-length. (c) Raw ZVH data for all heating shots showing differences in Cu k-α & k-β yield & shape. (d) Integrated Cu spectra (k-α:k-β) showing increase in temperature with increasing laser pulse length and decreasing distance from hemi to Cu sample.

A very successful day was completed with 13 shots (1 diagnostic calibration + 12 heating). A preliminary look at the data indicates that heating was optimal at longer laser pulse lengths (6 or 10 ps) and highest when the CH tamping surrounding the Cu samples was removed as evidenced by the appearance of higher charge states, as seen in the shaded region of Fig (c). Data analysis is ongoing, where detailed spectral analysis and PIC modeling will enable quantitative temperature measurements.

[1] P. K. Patel, et al., Phys. Rev. Lett. **91**, 125004 (2003).